Lambda Hyperon Production Mechanisms and Longitudinal Spin Transfer at HERMES[1]

Hsin Cynthia Chiang
Department of Physics
University of Illinois at Urbana-Champaign
Urbana, IL 61801

Advisor: Professor Naomi Makins, UIUC

April 15, 2003

[1]University of Illinois at Urbana-Champaign Department of Physics Senior Thesis

Abstract

It has been proposed that longitudinal spin transfer through the fragmentation process may be studied by examining Λ particles produced in the current fragmentation region. In order to correctly interpret spin-transfer data, the contribution of heavier hyperons such as Σ^* and Σ^0 to the production of Λ particles must be understood. In this study, events generated from a Monte Carlo simulation were used to examine Λ production mechanisms and to construct simple models for the longitudinal spin-transfer coefficient $D_{LL'}^{\Lambda}$. Comparisons were made between the simulations and data from the HERMES experiment. The simulations indicate that 40% to 60% of Λ particles are produced from heavier hyperons. More importantly, the simulations also indicate that very few Λ particles contain the polarized struck quark (about 10% on average), thus explaining the small degree of spin transfer observed at HERMES.

Contents

1 Introduction and background

1.1 Particle physics and the mystery of hadron structure

The aim of particle physics is to study the fundamental constituents of matter. Many particles have held the status of being "fundamental" at various points in history. For example, the atom was once thought to be the smallest unit of matter, but later it was discovered that atoms have internal structure and are composed of "fundamental" electrons, protons, and neutrons. Now it is known that protons and neutrons are also not fundamental particles; they are made of even smaller particles called *quarks*. All of the particles currently believed to be fundamental (quarks and leptons) are summarized in Table 1.1. In addition, each quark and lepton has an associated antiparticle. Finally, there are four more particles known as *vector bosons* that are associated with three fundamental forces (see Table 1.2).

The electromagnetic and weak forces are described by quantum electrodynamics (QED), and the strong force is described by quantum chromodynamics (QCD). These two theories and the descriptions of quarks and leptons comprise the *standard model*, which governs all of particle physics. By mixing and matching quarks in accordance with the rules of the standard model, it is possible to build a large number of particles known collectively as *hadrons*. For example, the proton is composed of two up quarks and one down quark, and the neutron is composed of one up quark and two down quarks. Protons and neutrons form a group of particles called *nucleons*, since they are the particles that make up atomic nuclei. More generally, any particle made of three quarks is known as a *baryon*. Nucleons are specific types of baryons; there are also other sub-categories of baryons. For example, *hyperons* are baryons that contain a strange quark. Another possible way of combining quarks to create a particle is by joining a quark and an antiquark; these particles are known as *mesons*.

Table 1.1: Fundamental particles in the standard model

Quarks		**Leptons**	
Up	Down	Electron	Electron neutrino
Charm	Strange	Muon	Muon neutrino
Top	Bottom	Tau	Tau neutrino

Table 1.2: Fundamental forces and associated vector bosons

Fundamental force	**Associated vector boson**
Electromagnetic	Photon
Weak	W boson
Weak	Z boson
Strong (nuclear)	Gluon

If it were possible to look inside a nucleon, for example, one might expect to see just the three main constituent quarks, also known as *valence quarks*. However, these are not the only quarks present—there are also short-lived quark–antiquark pairs that fluctuate in and out of the vacuum. These pairs are called *sea quarks*. Gluons, which carry the strong force, are exchanged between the quarks. Quantum chromodynamics should be able to describe the structure of all hadrons; however, several factors make QCD calculations difficult. Unlike the electromagnetic force, the strong force increases with distance, causing quarks to exist only in bound states. Quark bound states are highly relativistic; for example, nucleon binding energy is approximately 150 MeV. Confinement and the relativistic nature of quark bound states eliminate the possibility of using perturbation theory, so the details of hadron structure are presently still incalculable from first principles.

In order to solve some of the mysteries of hadron structure, the properties of constituent quarks must be examined to determine how they control the overall properties of a particle. Looking at the electric charge of the proton as an example, a proton has electric charge of $+1$, and its valence quarks, two ups and one down, have electric charges of $+2/3$ and $-1/3$ respectively. Adding these together, $2/3 + 2/3 - 1/3 = +1$. Gluons are neutral particles, and it is reasonable to assume that the charges of the sea quarks in the proton cancel each other, so it appears that the charge of the proton has been accounted for. Taking spin as a second example, it is conceivable that two of the valence quarks have oppositely aligned spins and that the spins of the sea quarks and gluons average out to zero, leaving behind one spin-1/2 valence quark that determines the spin of the overall proton. However, the European Muon Collaboration (EMC) showed in 1988 that, surprisingly, almost none of the nucleon's spin comes from its constituent quarks ("The Spin Crisis") [1]. Further experiments have shown that the up and down sea quarks in nucleons contribute little to the overall spin [2, 3], but not much is known about the gluon and strange quark contributions.

1.2 Introduction to deep-inelastic scattering

One method of investigating hadron structure is deep-inelastic scattering (DIS) of high energy lepton beams from nuclear targets. Deep-inelastic scattering was first demonstrated in a historic electron-scattering experiment conducted at the Stanford Linear Accelerator (SLAC) in the late 1960's [4]. At sufficiently high energies, electrons scattering from

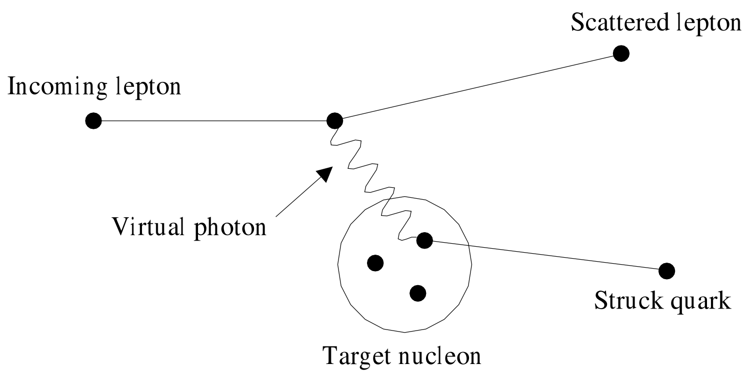

Figure 1.1: Deep-inelastic scattering schematic. The incoming lepton transfers momentum to one of the quarks in the target nucleon by emitting a virtual photon. The quark that absorbs the virtual photon is ejected from the nucleon and becomes one of the constituents of a new hadron.

protons no longer scatter from the protons as a whole, but instead scatter elastically from individual quarks—this phenomenon is known as *scaling*. A DIS event can be visualized as the exchange of a virtual photon between the beam lepton and the target nucleon (Figure 1.1). A summary of variables used to describe DIS events is provided in Table 1.3 [5].

The quark sub-structure of the nucleon is described by *parton distribution functions*, denoted $q(x)$. The Bjørken scaling variable x is a measure of the fractional momentum of the nucleon that the struck quark carries; $q(x)$ is the probability distribution for finding a quark of flavor $q = u, d, s$ at a particular value of x. In addition to carrying momentum, quarks inside the nucleon also carry spin. The spin distribution of the nucleon is described by *polarized parton distribution functions* $\Delta q(x)$, which describe the extent to which the spins of constituent quarks point in the same direction as the nucleon itself. It is possible to express $q(x)$ and $\Delta q(x)$ in terms of the average number of spin-up and spin-down quarks, $\langle \hat{n}_{q^\uparrow}(x) \rangle$ and $\langle \hat{n}_{q^\downarrow}(x) \rangle$:

$$q(x) \equiv \langle \hat{n}_{q^\uparrow}(x) \rangle + \langle \hat{n}_{q^\downarrow}(x) \rangle$$
$$\Delta q(x) \equiv \langle \hat{n}_{q^\uparrow}(x) \rangle - \langle \hat{n}_{q^\downarrow}(x) \rangle.$$

Polarized lepton beams can be used to study the spin structure of the nucleon. If the incoming lepton is polarized, the virtual photon emitted is also polarized. Only the quarks with spin antiparallel to the beam can absorb the virtual photon; therefore, the use of a polarized beam selects quarks with a particular spin direction and thus effectively produces a beam of polarized quarks (Figure 1.2).

When the target nucleon is broken apart in a DIS event, the struck quark speeds away from the target remnant with a large momentum. As the distance between the struck quark and target remnant increases, the strong force between them increases to the point where it is energetically favorable for a quark–antiquark pair to be pulled out of the vacuum. The process of creating quark–antiquark pairs continues until the relative momenta

Table 1.3: Variables used to describe DIS events

Variable	Definition	Description
$\vec{k}$	$(E, \vec{p})$	Four-momentum of incoming lepton
$\vec{k}'$	$(E, \vec{p}')$	Four-momentum of scattered lepton
$\vec{P}$	$(M, 0, 0, 0)$	Four-momentum of target nucleon
$\vec{P}_h$	$(E_h, \vec{p}_h)$	Four-momentum of outgoing hadron
$\vec{q}$	$\vec{k} - \vec{k}'$	Four-momentum of virtual photon
Q^2	$-q^2$	Negative squared four-momentum transfer
ν	$E - E'$	Energy transfer
y	$\frac{\nu}{E}$	Relative energy transfer
x	$\frac{Q^2}{2M\nu}$	Bjørken scaling variable
W^2	$M^2 + Q^2(\frac{1}{x} - 1)$	Invariant mass of final hadronic state
z	$\frac{E_h}{\nu}$	Fractional hadron energy

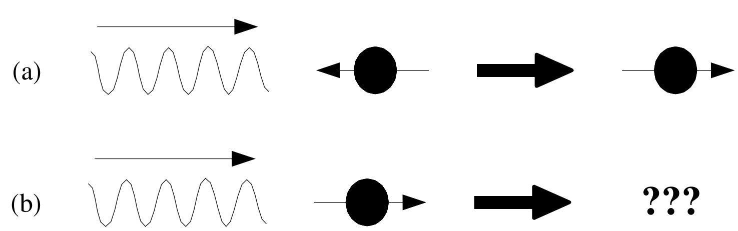

Figure 1.2: In (a), a spin-1 virtual photon and spin-1/2 quark are oppositely aligned. The quark is able to absorb the photon and change polarization. In (b), if the quark were to absorb the photon, the end result would be a quark with spin-3/2, which cannot exist.

of the quarks has sufficiently decreased; the quarks and antiquarks then coalesce to form observable hadrons. This process of forming observable hadrons from struck quarks is known as *hadronization* or *fragmentation*. Fragmentation is a highly non-perturbative QCD process and is presently very poorly understood. In particular, little is known about longitudinal spin transfer between the original struck quark and the final hadron that contains that quark, i.e. the extent to which the spin of the struck quark determines the spin of the final hadron.

When performing a DIS experiment, the measurement can be *inclusive*, where a single particle in the final state is detected, or *semi-inclusive*, where two or more final particles are detected. The differential cross section for producing a hadron h in an unpolarized semi-inclusive DIS event is

$$d\sigma^h \sim \sum_q e_q^2 \, q(x) \, D^{q/h}(z).$$

Here the sum is over the three quark flavors $q = u, d, s$; e_q is the charge of the struck quark, $q(x)$ is the parton distribution function, and $D^{q/h}(z)$ is the fragmentation function, which describes the probability for a quark q to fragment into a hadron h carrying energy fraction z.

1.3 The HERMES experiment

HERMES is a nuclear physics experiment devoted to studying the spin structure of the nucleon using semi-inclusive DIS. It is one of four experiments located at the Deutsches Elektronen-Synchrotron (DESY), a particle accelerator facility in Hamburg, Germany. The main storage ring, HERA, has a circumference of 3.9 miles and contains an 820-GeV proton beam and a 27.6-GeV positron beam. As the positrons circle around the ring, they emit synchrotron radiation and become naturally transversely polarized due to the Sokolov–Ternov effect [6]. HERMES uses only the polarized positron beam and passes it through spin rotators so that the polarization is changed from transverse to longitudinal. The longitudinally polarized beam strikes a gas target; targets that have been used in the past include polarized hydrogen, deuterium, helium, and various heavier unpolarized gases.

The HERMES spectrometer consists of a number of detectors. Drift chambers are used to determine charged particle trajectories and are used in combination with a magnet to determine particle momenta. A lead glass calorimeter, scintillator hodoscope, and transition radiation detector are used to identify hadrons and leptons. Further particle identification (PID) is achieved with the Ring Imaging Cherenkov (RICH). The RICH is able to separate pions, kaons, and protons by measuring the angle of the Cherenkov cone emitted when these particles enter the detector. A complete description of the HERMES spectrometer is provided in reference [7].

1.4 Probing spin transfer via Λ particles

The main focus of the research presented in this thesis is understanding longitudinal spin transfer through the fragmentation process. One technique for studying spin transfer

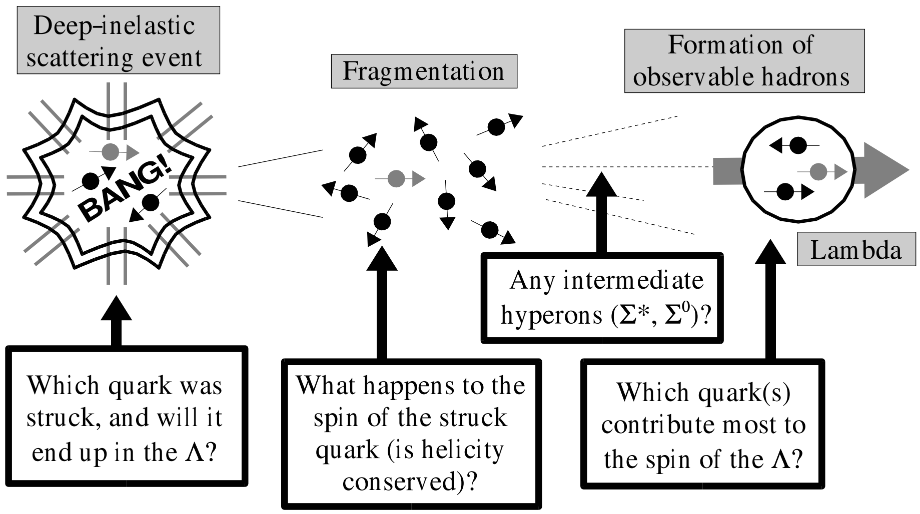

Figure 1.3: Diagram of the main factors that influence our knowledge of $D^{\Lambda}_{LL'}$. The only piece of information in this picture that can be obtained directly from experiment is the final spin of the Λ.

is examining the production of Λ particles in DIS events [8, 9]. The Λ is composed of an up, down, and strange quark, and decays via the parity-violating weak interaction; therefore it is possible to deduce the spin of the Λ (on average) by measuring the angular distribution of its decay products. The naïve constituent quark model predicts that the spin of the Λ is determined by the strange quark alone ($\Delta u_{\Lambda} = \Delta d_{\Lambda} = 0$, $\Delta s_{\Lambda} = 1$). By examining DIS events in which Λ particles originated from the struck quark (*current fragmentation*), it may be possible to use the Λ as a probe for understanding spin transfer through the fragmentation process. We are interested in measuring the longitudinal spin transfer coefficient $D^{\Lambda}_{LL'}$, which depends on (1) the spin structure of the Λ, (2) subprocesses that contribute to the production of Λ particles, and (3) the degree to which helicity is conserved in the fragmentation process (see Figure 1.3).

Longitudinal spin transfer to Λ particles has previously been studied by the ALEPH [10] and OPAL [11] collaborations, which examined the decays of Z bosons produced in electron–positron scattering events. Both collaborations were able to successfully model their spin-transfer data by using Monte Carlo simulations to determine subprocess fractions for Λ production, and calculating the degree of spin transfer in each subprocess. Two simple assumptions [12] were made in order to model the spin-transfer data:

- Helicity is perfectly conserved during fragmentation.
- Quarks produced during fragmentation have random polarizations (i.e. only hyperons containing the struck quark are polarized).

In contrast to ALEPH and OPAL, HERMES examines Λ particles produced in polarized deep-inelastic lepton scattering. Data on spin transfer have been collected; these data relate $D^{\Lambda}_{LL'}$ to z, the fraction of available energy that is carried by the Λ particle (Figure 1.4).

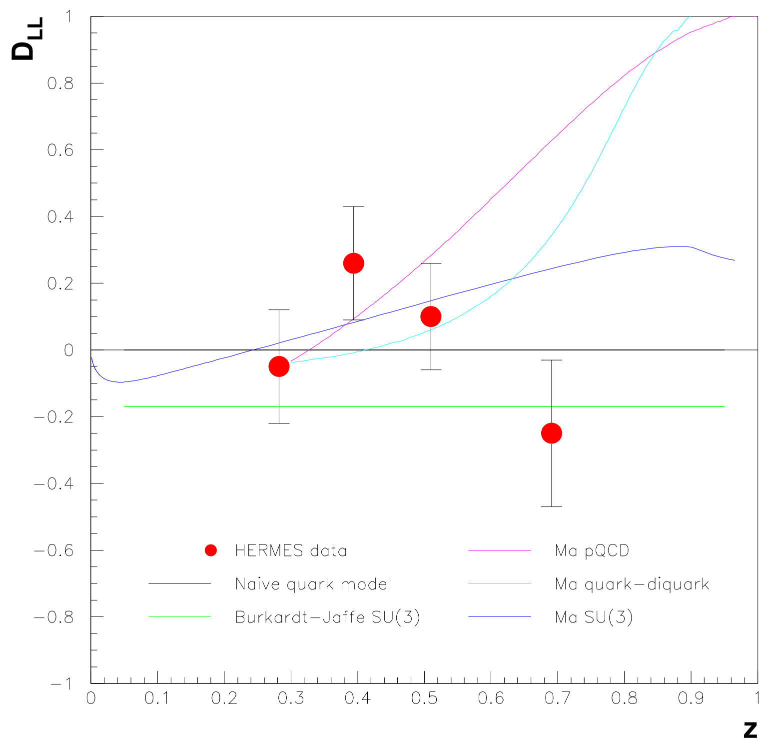

Figure 1.4: Plot of $D_{LL'}^{\Lambda}$ versus z, where $D_{LL'}^{\Lambda}$ is the longitudinal spin-transfer coefficient and z is the fractional available energy carried by Λ particles. The red points represent HERMES data taken in the years 1996-2000, and the lines represent the predictions of two naïve models and three more sophisticated calculations [13, 14].

The spin-transfer data is shown in comparison with five different models, all of which assume that the Λ particles are produced directly from the struck quark. The first model is the naïve constituent quark model, which predicts that the spin of the Λ is determined by the strange quark alone and that $D_{LL'}^{\Lambda}$ is therefore zero. The second model examines existing data on hyperon decays and polarized parton distribution functions, and uses SU(3) symmetry to predict that there is a small, non-zero contribution from up and down quarks to Λ spin [8]. In addition to the two simple models, more sophisticated calculations of the Λ parton distribution functions have been performed in references [13, 14]. These calculations agree that $D_{LL'}^{\Lambda}$ rises as a function of z.

It is particularly surprising that the largest discrepancy in Figure 1.4 lies between the data and the models that attempt to calculate the z-dependence of $D_{LL'}^{\Lambda}$. One possible explanation for the discrepancy is that, contrary to the model assumptions, not all Λ particles are produced directly from the current fragmentation process. A Λ can also be produced as a decay product of a heavier hyperon such as Σ^* or Σ^0; thus examining the spin structure of a decay Λ reflects the spin structure of its parent [12]. Monte Carlo studies have indicated that Σ^* and Σ^0 particles make significant contributions to Λ production (29% and 18%, respectively [5]); therefore, it is impossible to proceed with analysis of spin transfer data without first studying and understanding the Σ^* and Σ^0 contamination.

The aim of this study is to construct a Monte Carlo model of $D_{LL'}^{\Lambda}$ at HERMES, using the simple hypotheses of the ALEPH and OPAL papers. From this study, we hope to arrive at a better understanding of the dominant Λ-production mechanism at HERMES and resolve the apparent discrepancy between the small spin transfer we observe, the large values measured at LEP, and the available theoretical calculations.

2 Comparison of hyperon yields in Monte Carlo and data

2.1 Generating Monte Carlo events

In this study, Monte Carlo simulations are used to calculate the fraction of Λ particles produced from the decay of heavier hyperons. To verify the accuracy of the Monte Carlo, it is necessary to compare the relative yields of fully reconstructed Λ, Σ^*, and Σ^0 resonances in the data and Monte Carlo.

Monte Carlo simulations are important for several reasons. In contrast to real data, all of the identities of the generated particles are known. This knowledge makes it is possible to optimize *cuts*, which are restrictions that are imposed in order to identify events of interest. (An example of a simple cut that might be used to identify an electron is requiring that the charge be negative.) The simulations also make it possible to perform background subtractions and check that the analysis code is working correctly. There are four main steps[1] in the simulation process:

- Randomly generate physics events based on known cross-sections.
- Simulate HERMES detector responses to the generated events.
- Reconstruct track information from simulated detector responses.
- Output track information in a format identical to the data.

It is fairly rare that a Λ (and its parent) are present in the data and can be reconstructed. The efficiency of the Monte Carlo simulation in producing events of interest can be greatly increased by applying a *selector*, which places various restrictions on generated events. (Unwanted events are discarded, but counted for normalization purposes.) The set of Monte Carlo samples that was generated for comparison to the data contains particles that mimic the decay products of the Λ and reconstruct to an invariant mass close to $M_\Lambda = 1.116$ GeV$/c^2$. At least two tracks were required to be in each event—a negatively-charged hadron (μ^-, π^-, K^-, or $\bar{p}$) mimicking a pion from a Λ, and a positively-charged hadron (μ^+, π^+, K^+, or p) mimicking a proton from a Λ. These two tracks were required

[1]Generator Monte Carlo (GMC), HERMES Monte Carlo (HMC), HERMES Reconstruction Code (HRC), and the data summary tape writer (writeDST).

to have a momentum greater than 0.2 GeV/c and to be in the acceptance of the HERMES spectrometer:

$$0.000\,\text{mrad} < \theta_x < 0.200\,\text{mrad}$$
$$0.020\,\text{mrad} < \theta_y < 0.170\,\text{mrad}.$$

The tracks were also required to reconstruct to an invariant mass between 1.005 GeV/c^2 and 1.135 GeV/c^2. A total of 400000 Monte Carlo events (27285784 generated events) were used for comparison to the data.[2]

2.2 Overview of applied cuts for Λ candidates

Figure 2.1 shows the flowchart of the analysis code used to find Λ, Σ^*, and Σ^0 candidates in data and Monte Carlo. The data used was from the 2000 run of HERMES (2000b1 production); no data quality cuts have been implemented.

Events that contain Λ candidates must be identified before attempting to find Σ^* and Σ^0 candidates. Lambda particles are relatively long-lived (lifetime at rest, τ, is approximately 2.632×10^{-10} seconds, $c\tau \simeq 7.89$ cm). However this lifetime is still too short for Λ particles to be detected directly by any of the HERMES detectors; therefore, it is necessary to search for the Λ decay products. Lambda particles decay via $\Lambda \to p + \pi^-$ with a 63.9% branching ratio[3], as shown in Figure 2.2.

In order for an event to contain a Λ candidate, that event must have had at least three tracks: the scattered positron, a proton, and a negative pion. Combined detector responses were used to separate hadrons from leptons.[4] All positive hadrons were assumed to be protons, and all negative hadrons were assumed to be pions. (As described later in Section 2.7, the RICH was found to be unnecessary.) Low-momentum negatively-charged particles that did not reach the end of the HERMES spectrometer (i.e. short tracks that did not reach the PID detectors) were assumed to be pions if they had momentum below 2 GeV. The scattered positron was required to have originated from the target cell (-20 cm $< z <$ 20 cm), and a cut was made on the radial separation between the track and the beam axis ($r < 0.75$ cm). In addition, the following kinematic cuts were made to ensure that the positron came from a DIS event:

$$1 < Q^2 < 24$$
$$y < 0.85$$
$$W^2 > 4.$$

[2]Events were generated using gmc_disNG with parameters tuned by Felix Menden, 1997 geometry file, and NOVC tracking.

[3]The Λ has several other decay modes, including $\Lambda \to n+\pi^0$ (35.8% branching ratio). Lambda candidates were not identified using this decay mode because the HERMES spectrometer cannot track neutral particles.

[4]PID3 + PID5 > 0 for leptons, and PID3 + PID5 < 0 for hadrons.

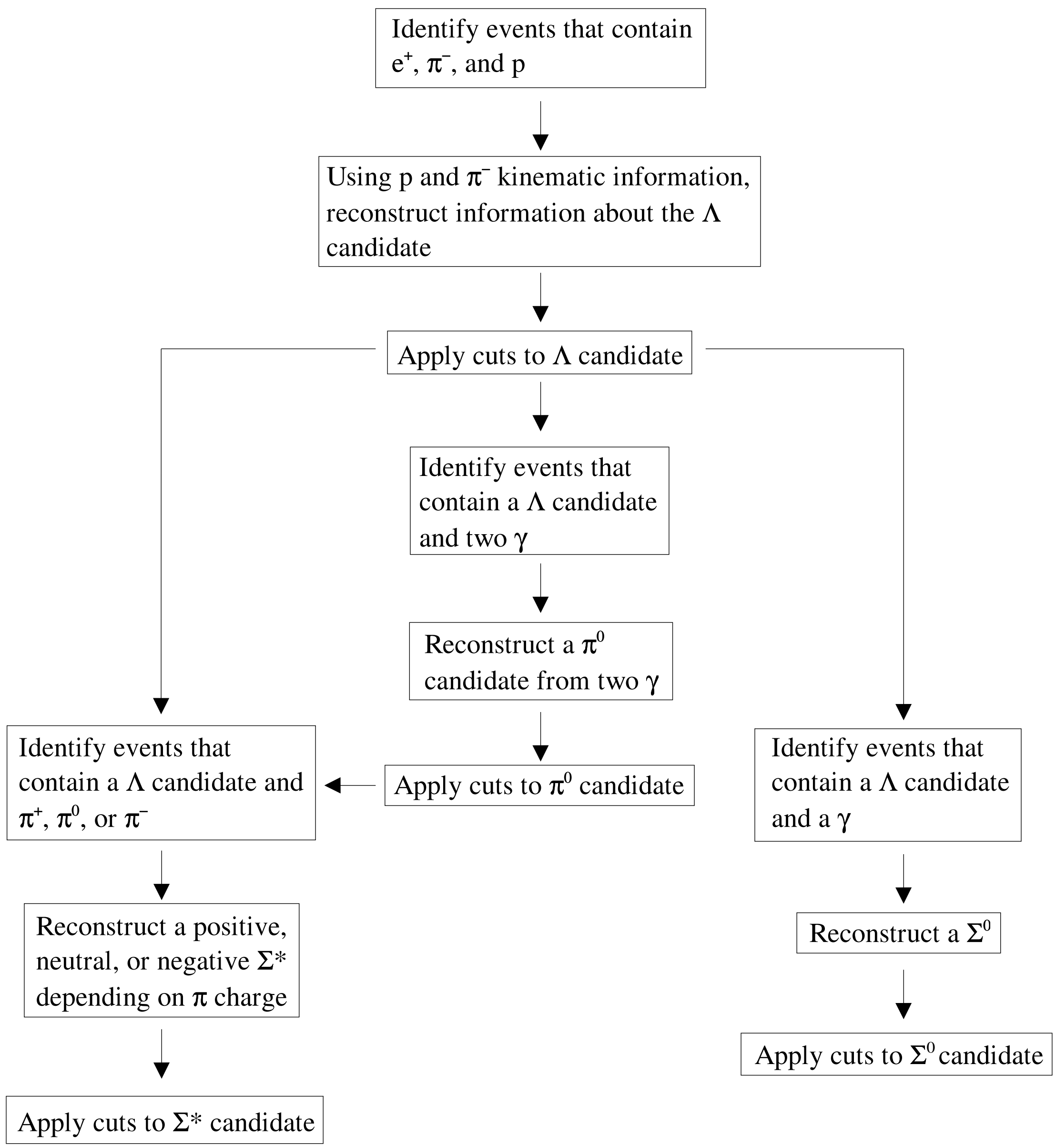

Figure 2.1: Flowchart of analysis code used to identify Σ^* and Σ^0 particles in HERMES data. Events are examined first for the presence of Λ candidates and then for the presence of Σ^* and Σ^0.

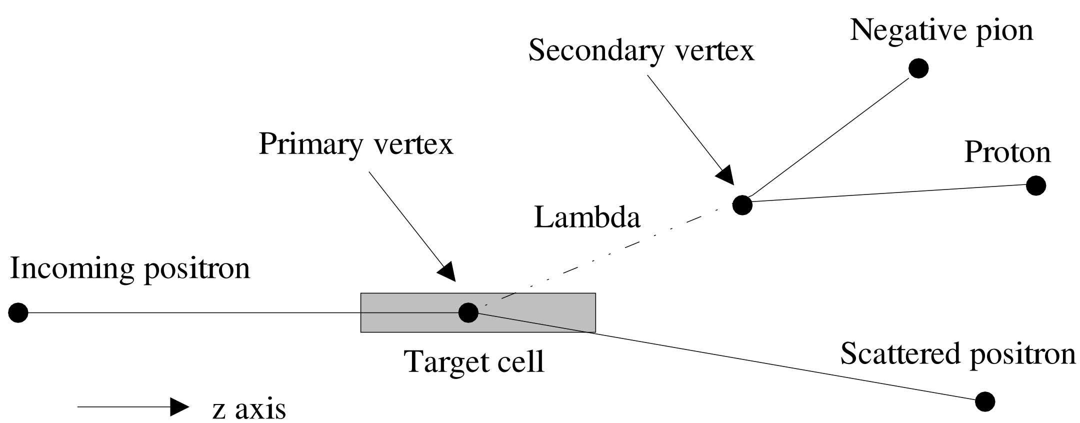

Figure 2.2: Deep-inelastic scattering event resulting in the production of a Λ that decays to a proton and negatively charged pion. The Λ is neutral and cannot be detected directly; only the decay products and the scattered positron can be detected.

The cut on Q^2 ensures that the reaction is in the scaling regime, the cut on y reduces the need for radiative corrections, and the cut on W^2 decreases the likelihood for events to contain target resonances (e.g. the Δ resonance of the proton). If more than one particle in an event satisfied these criteria, the positron with the highest momentum was selected.

The proton momentum was required to be greater than the pion momentum; Monte Carlo studies reveal that this kinematic correlation holds for all Λ particles detected at HERMES. The distance of closest approach between the negative pion and the proton tracks was required to be less than 1.5 cm, and the secondary vertex was determined by the midpoint between the two tracks.[5] Because the Λ decays weakly and is long-lived, the distance between the primary and secondary vertices was required to be greater than 5 cm. There are two ways to calculate the trajectory of the Λ candidate. Its momentum $\vec{P}_\Lambda$ can be reconstructed by adding the momentum vectors of its decay products, or a spatial vector $\vec{S}$ can be formed between the primary and secondary vertices. Clearly, $\vec{S}$ and $\vec{P}_\Lambda$ must be parallel. A collinearity cut was imposed using these two vectors:

$$\frac{\vec{P}_\Lambda \cdot \vec{S}}{P_\Lambda S} > 0.9995.$$

If an event with a Λ candidate satisfied all the above criteria, the Λ candidate's energy and momentum were reconstructed from the child particles, and the invariant mass was calculated. It is relatively easy to obtain a clean Λ peak at the correct invariant mass, 1.116 GeV/c^2.

2.3 Overview of applied cuts for Σ^* and Σ^0 candidates

Events that contain Λ candidates can be examined further to see if they contain any Σ^* or Σ^0 candidates. Σ^* and Σ^0 particles decay via the following mechanisms:

$$\Sigma^* \to \Lambda + \pi$$
$$\Sigma^0 \to \Lambda + \gamma.$$

The branching ratios are 88% and 100%, respectively. One of the main reasons that Σ^* particles are difficult to detect is that the child pions often have fairly low momenta and are outside the acceptance of the HERMES spectrometer. Similarly, Σ^0 particles are difficult to detect because photons are neutral particles and leave no track information; they leave only untracked clusters in the calorimeter. Both Σ^* and Σ^0 particles are extremely short-lived and decay inside the target cell, so there are few cuts that can be made in comparison to Λ candidates (for example, no collinearity or vertex-separation cuts can be made).

[5] It is more accurate to determine the vertex using an error matrix given by the uncertainty in each track. However, according to reference [5], the accuracy lost by using the midpoint method is negligible.

The Σ^* candidates were identified in a manner similar to Λ particles. Events with Λ candidates were examined for the presence of positive, negative, or neutral pions, and all possible pairs were formed between Λ candidates and pions. (In the case of neutral Σ^* particles, the neutral pions were first reconstructed from two photons). The child pion was required to have originated from the target cell, and the radial separation between its track and the beam axis was required to be less than 5 cm. A cut was also made on the invariant mass of the child Λ particle: 1.08 GeV/c^2 $<$ mass $<$1.15 GeV/c^2. Finally, a multiplicity cut was made on the number of Σ^* candidates per event. It is possible, but highly unlikely, that one DIS event produces more than one Σ^* particle, so any events containing more than one Σ^* candidate were discarded.

Compared to Σ^* particles, there are even fewer cuts that can be applied to Σ^0 candidates, since there is no track information for the child photon. Photon hits in the calorimeter were assumed to have originated at the vertex of the scattered beam positron, and this information was used to calculate the photon's momentum components. The photon energy was required to be less than 1.5 GeV, and the same multiplicity cut used for Σ^* identification was used for the Σ^0 candidates, i.e. no more than one candidate per event.

2.4 Searching for Λ

A clean Λ invariant mass peak can be obtained in the Monte Carlo and data without using hadron PID (see Figure 2.3). It should be noted that the signal-to-background ratio appears lower in the data than in the Monte Carlo. This discrepancy indicates that the Monte Carlo parameters need tuning; it is unclear how the difference in Λ yields affects this analysis. A second difference between the Λ signal in the Monte Carlo and data is the width of the peak ($\sigma_{\mathrm{data}} = 0.00253 \pm 0.00004$, $\sigma_{\mathrm{mc}} = 0.00175 \pm 0.00005$). There are two possible reasons for this difference. First, the addition of the RICH has degraded the resolution of the HERMES spectrometer, and the Monte Carlo used in this study does not account for this effect. Second, because the Monte Carlo samples were generated using a selector, the Λ itself was not tracked through the spectrometer. There may therefore be some smearing of the Λ tracks in the data that is not present in the Monte Carlo.

A plot of the Monte Carlo Λ mass spectrum separated into background and true Λ particles is shown in Figure 2.4. Because the background level is low and approximately linear, it is possible to perform background subtraction using the sideband method (see Figure 2.5). In this method, the invariant mass spectrum is integrated in three mass windows—a 3σ window containing the central peak, and two windows (sidebands) of the same width on either side of the peak. The sidebands are averaged and subtracted from the central peak in order to obtain the true number of signal counts. It is also possible to perform background subtraction by fitting a curve to the invariant mass spectrum. In Figure 2.6, the background is fit with a first-order polynomial, and the signal is fit with a gaussian. The fit parameters and χ^2 per degree of freedom (χ^2/ndf) are listed in Table 2.1. The number of signal counts is obtained by integrating the gaussian and dividing by the histogram bin width.

The number of Λ candidates in the data and Monte Carlo was calculated using both the sideband and curve fit methods. The sideband method was more accurate and produced

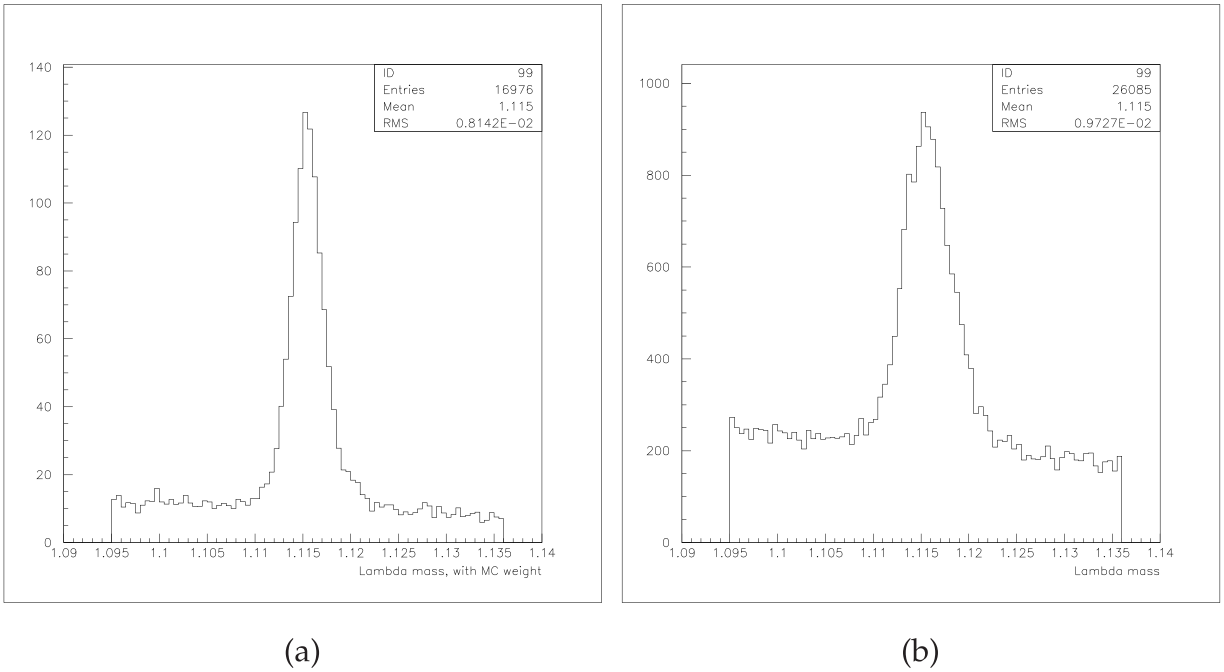

Figure 2.3: Lambda invariant mass (GeV/c^2) spectra for (a) Monte Carlo and (b) data. No hadron PID was used to obtain these spectra.

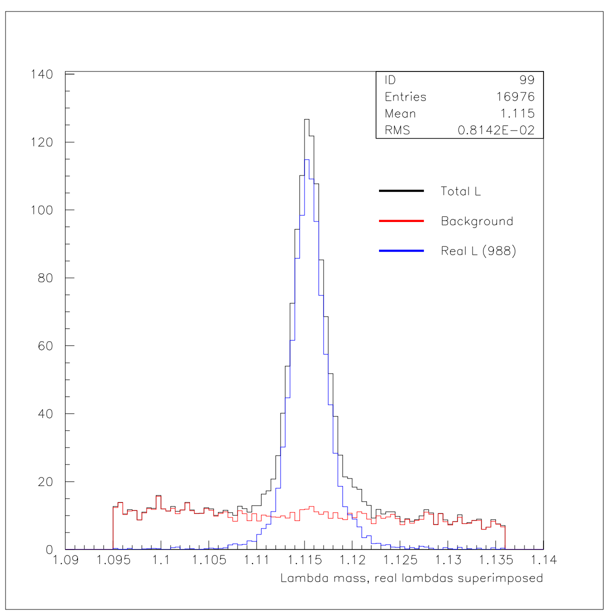

Figure 2.4: Lambda invariant mass (GeV/c^2) spectrum for Monte Carlo. The red line indicates the background, and the blue line indicates "real" Λ particles.

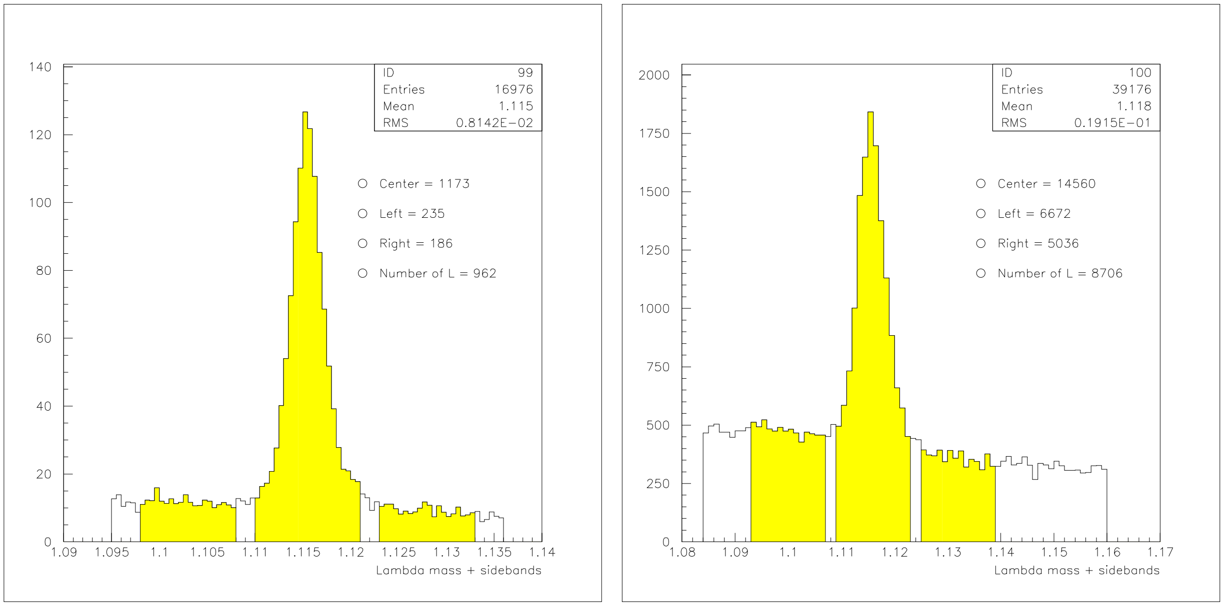

(a) (b)

Figure 2.5: Lambda invariant mass (GeV/c^2) spectra for (a) Monte Carlo and (b) data. The sidebands and central peak used for background subtraction are indicated by the hatched regions. The number of Λ counts after background subtraction is 982 ± 38 in the Monte Carlo, and 8706 ± 132 in the data.

Table 2.1: First-order polynomial (P1) and gaussian (G) fit parameters for Λ invariant mass spectrum in Monte Carlo and data

	Monte Carlo	Data
P1: intercept	1.5 ± 0.5	2061 ± 24
P1: slope	7.8 ± 0.5	-1659 ± 21
G: amplitude	106 ± 4	687 ± 11
G: mean	1.1155 ± 0.00004	1.1157 ± 0.00003
G: sigma	0.00175 ± 0.00005	0.00253 ± 0.00004
χ^2/ndf	$36.60/77$	$102.7/77$

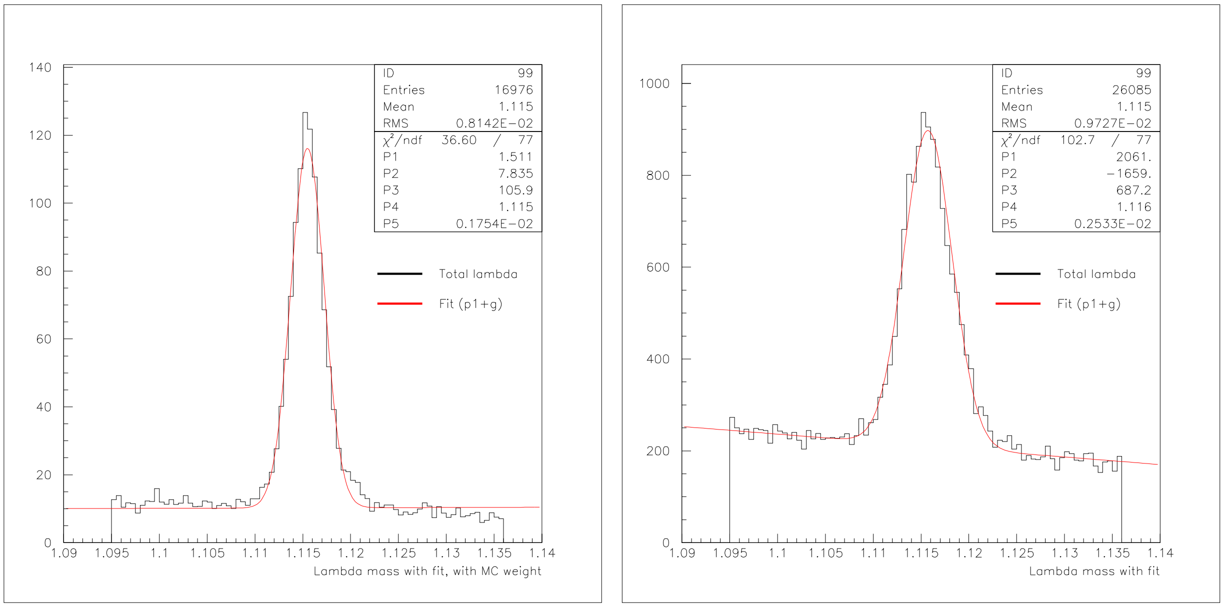

(a) (b)

Figure 2.6: Lambda invariant mass (GeV/c^2) spectra for (a) Monte Carlo and (b) data. A curve fit (indicated by the red line) consisting of the sum of a first-order polynomial and a gaussian was performed for each plot. The number of Λ counts obtained from integrating the gaussian is 931 ± 54 in the Monte Carlo, and 8725 ± 241 in the data.

Table 2.2: Number of Λ candidates reconstructed in Monte Carlo and data

	Monte Carlo	Data
Sideband subtraction	962 ± 38	8706 ± 132
Curve fit	931 ± 54	8725 ± 241
Actual number	988	—

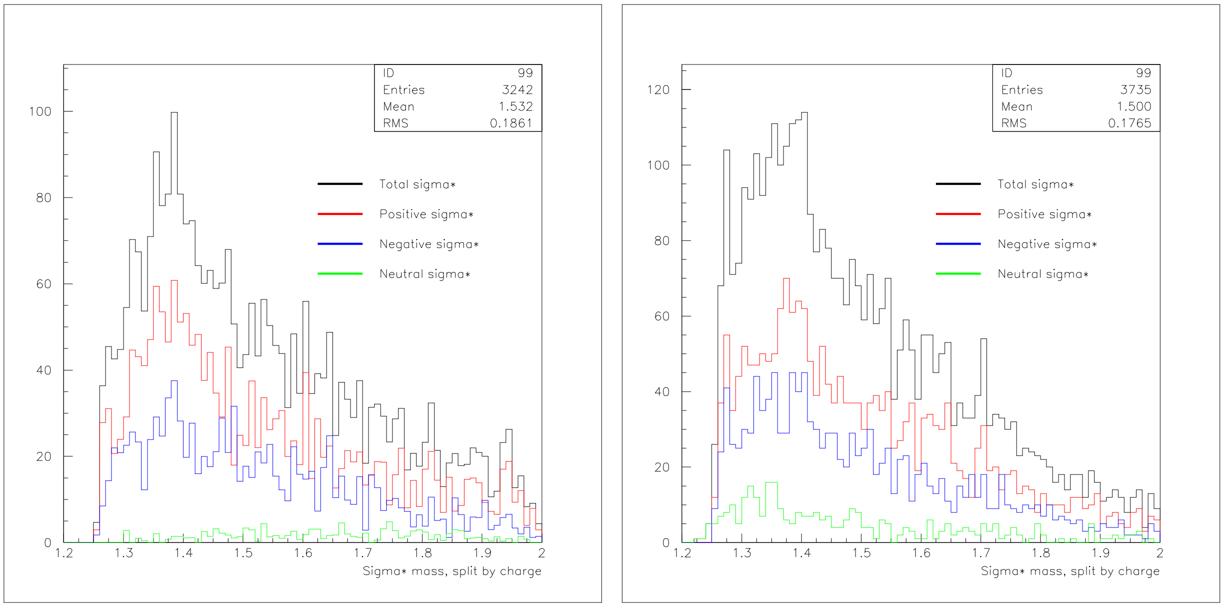

(a) (b)

Figure 2.7: Plot of Σ^* invariant mass (GeV/c^2) for (a) Monte Carlo and (b) data. The black, red, blue, and green lines indicate total, positive, negative, and neutral Σ^* respectively.

a number closer to the true number of Λ particles generated by the Monte Carlo (see Table 2.2). The sideband method was therefore chosen for calculating the number of Λ candidates in the data.

2.5 Searching for Σ^*

In contrast to Λ particles, it is difficult to obtain a visible Σ^* invariant mass peak. All results from the Σ^* search in the Monte Carlo were normalized to the data using the Λ yield: all Monte Carlo yields presented here were divided by the total number of Λ particles found in the Monte Carlo, and multiplied by the number of Λ particles in the data. Plots of the Σ^* invariant mass in the Monte Carlo and data are shown in Figure 2.7.

Because the signal from neutral Σ^* is not visible, it is omitted from the following analysis. It is necessary to study the Monte Carlo in order to understand the type of background beneath the small Σ^* signals; Figures 2.8 and 2.9 show Monte Carlo Σ^* mass plots separated into background and "real" Σ^* particles. These plots show that the shape of the background is more complicated than a first-order polynomial. A better fit to the background can be obtained by using a second-order polynomial ($A_0 + A_1x + A_2x^2$, where A_0, A_1, and A_2 are the free parameters), and the signal can be fit by a gaussian. Figure 2.10 shows fits to invariant mass plots for combined positive and negative Σ^* particles in the Monte Carlo and data. The fit parameters are listed in Table 2.3. The number of Σ^* particles can be obtained from the curve fit by integrating the gaussian and dividing by the

Table 2.3: Second-order polynomial (P2) and gaussian (G) fit parameters for combined positive and negative Σ^* invariant mass spectrum in Monte Carlo and data

	Monte Carlo	Data
P2: A_0	-508 ± 15	-462 ± 17
P2: A_1	875 ± 13	878 ± 14
P2: A_2	-336 ± 7	-353 ± 8
G: amplitude	27 ± 6	30 ± 7
G: mean	1.383 ± 0.005	1.387 ± 0.006
G: sigma	0.024 ± 0.006	0.020 ± 0.006
χ^2/ndf	$24.22/23$	$17.39/23$

Table 2.4: Number of combined positive and negative Σ^* candidates reconstructed in Monte Carlo and data

	Monte Carlo	Data
Curve fit	158 ± 55	148 ± 60
Actual number	148	—

histogram bin width. Table 2.4 lists the number of positive and negative Σ^* particles obtained from curve fits in the Monte Carlo and data.

Another method of performing background subtraction is using sidebands in the Λ mass spectrum to determine the level of background in the Σ^* mass spectrum. In this method, Λ candidates from the sidebands above and below the central Λ peak are used to reconstruct Σ^* candidates. There is a high probability that the sideband Λ candidates do not correspond to actual Λ particles, so they should reconstruct false Σ^* particles. The invariant mass spectra of the Σ^* candidates reconstructed from the Λ sidebands are averaged and scaled up to the level of the background in the overall Σ^* mass spectrum. However, as shown in Figure 2.11, this method of background subtraction works poorly because the Σ^* peak is near a kinematic edge in the invariant mass plot.

The combined positive and negative Σ^* invariant mass spectra in the data and Monte Carlo are in good agreement when a curve fit is used for background subtraction. It was not possible to obtain a stable fit for positive Σ^* and negative Σ^* individually due to low statistics.

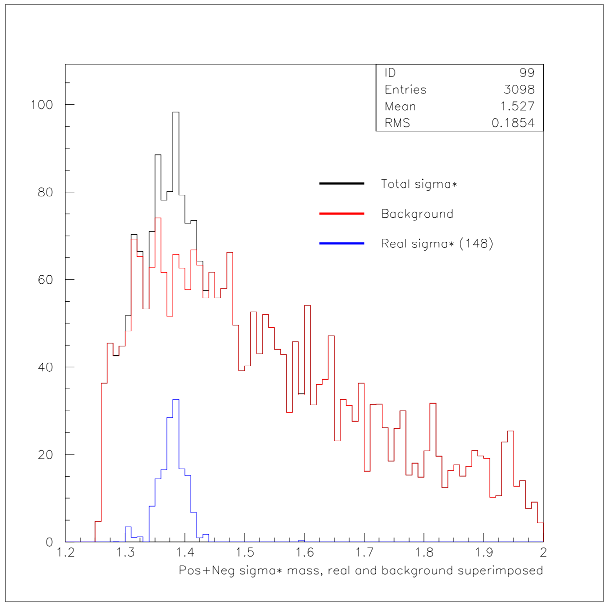

Figure 2.8: Plot of combined positive and negative Σ^* invariant mass (GeV/c^2) for Monte Carlo. The red line indicates the background, and the blue line indicates "real" Σ^* particles. There are 148 real positive and negative Σ^* particles.

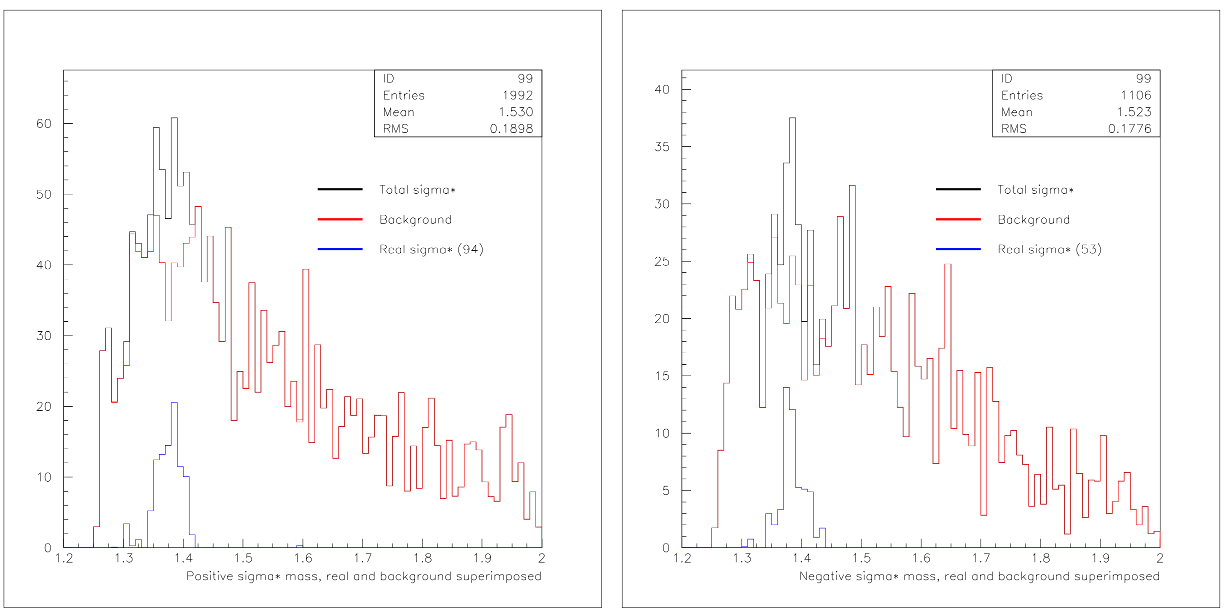

(a) (b)

Figure 2.9: Plot of (a) positive and (b) negative Σ^* invariant mass (GeV/c^2) for Monte Carlo. The red line indicates the background, and the blue line indicates "real" Σ^* particles. There are 94 real positive and 53 real negative Σ^* particles.

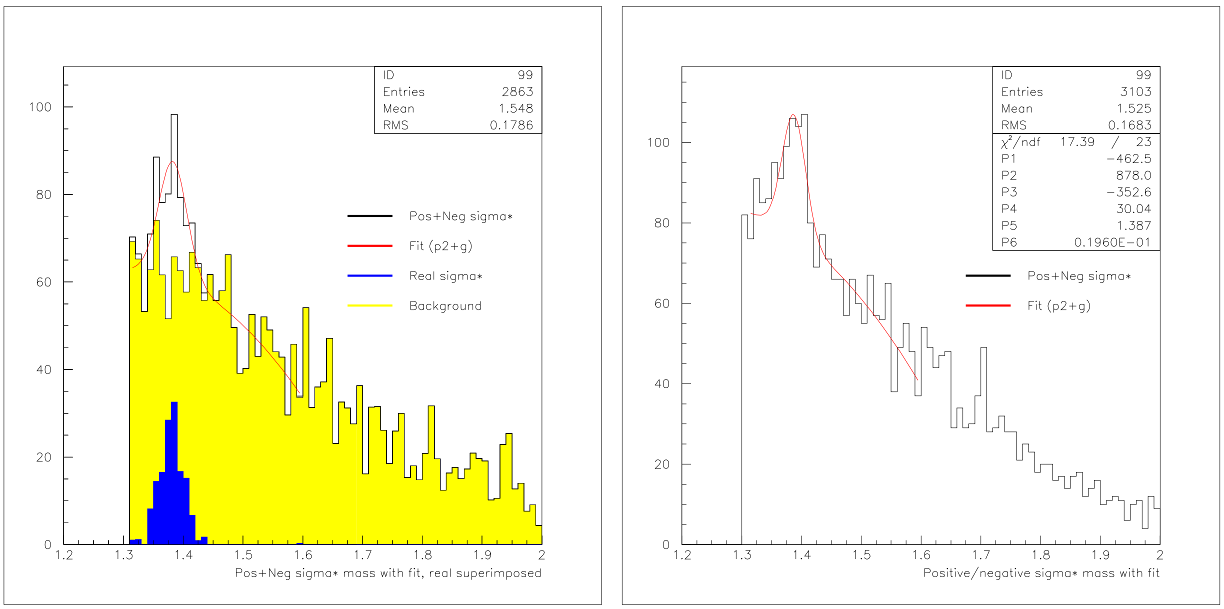

(a) (b)

Figure 2.10: Plot of combined positive and negative Σ^* invariant mass (GeV/c^2) for (a) Monte Carlo and (b) data. The red line indicates the curve fit in both plots. There are 158 ± 55 Σ^* particles in the Monte Carlo, and 148 ± 60 in the data. In (a) the blue region indicates "real" Σ^* particles, and the yellow region indicates background.

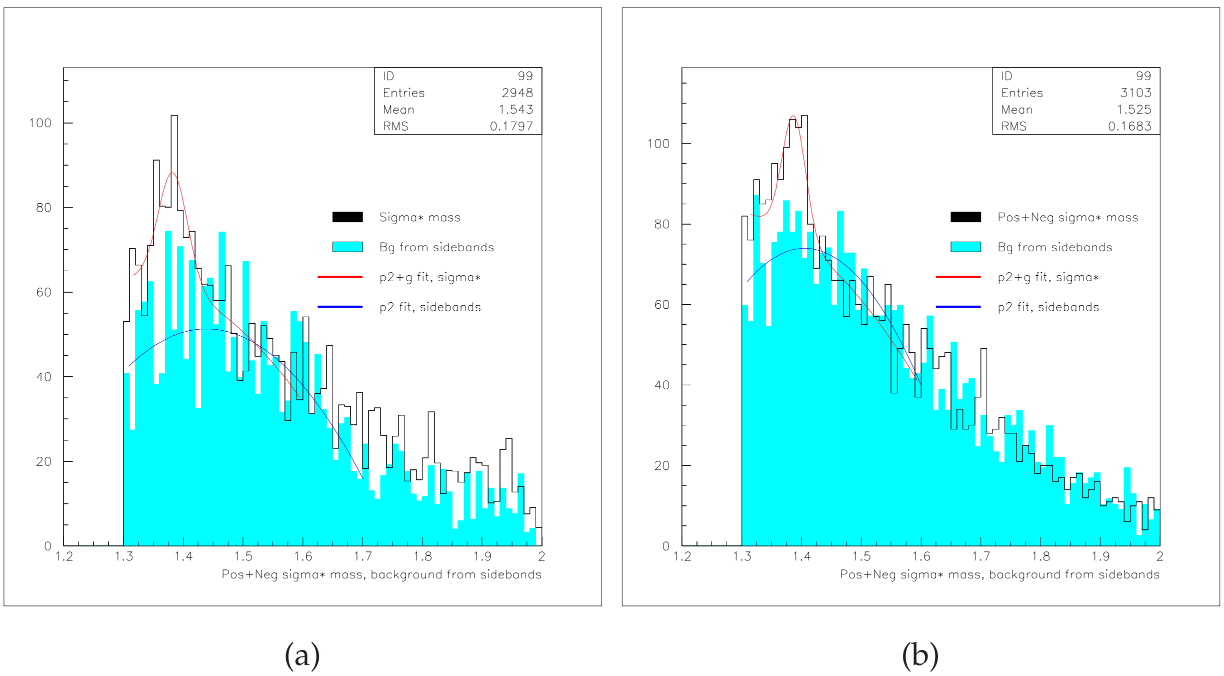

Figure 2.11: Plot of Σ^* invariant mass for (a) Monte Carlo and (b) data. Lambda sidebands are used to determine the level of the background (cyan region); overall curve fits (red) and background fits (blue) are shown. This method of background subtraction is not effective, since the Σ^* peak is near a kinematic edge in the invariant mass plot.

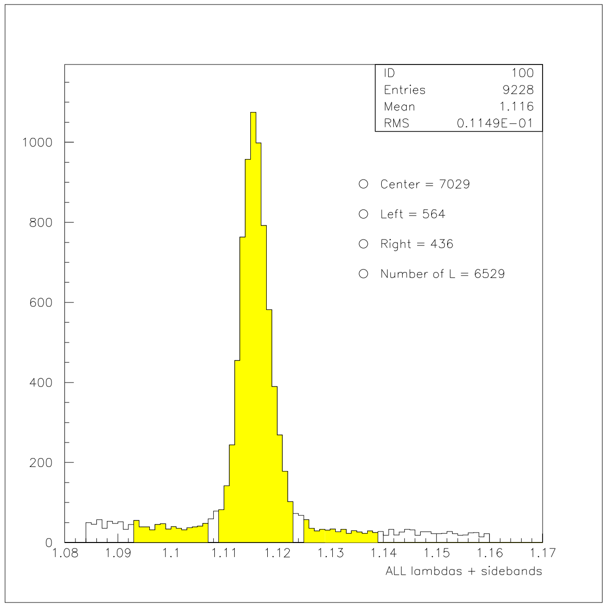

Figure 2.12: Lambda invariant mass spectrum taken from 2000b1 data using the RICH for hadron identification. Note that the background level is reduced in comparison with the mass spectrum taken using no hadron PID (Figure 2.5b); however, the total number of Λ candidates (6529 ± 85, using the sideband method for background subtraction) is also reduced.

2.6 Searching for Σ^0

A preliminary examination of the data indicates that the Σ^0 signal is overwhelmed by the background and is not visible. However, because it is currently not possible to trace the origin of photons produced in the Monte Carlo, it is very difficult to confirm this result. Further studies of the Σ^0 yield in the data and Monte Carlo are needed.

2.7 (Not) using the RICH

As previously mentioned, the above results were obtained using no hadron PID. The same analysis can be performed using information from the RICH detector, which is capable of separating protons, pions, and kaons. As shown in Figure 2.12, the RICH greatly reduces the background level in the Λ mass spectrum. However, the total number of Λ candidates after background subtraction is also reduced (8706 $\pm$ 132 without hadron PID, 6529 $\pm$ 85 with RICH). The decreased number of Λ candidates makes Σ^* reconstruction more difficult, and it is almost impossible to find a Σ^* peak in the data when the RICH is used (see Figure 2.13). It is unnecessary to use hadron PID given the powerful vertex-separation and collinearity cuts available in the Λ analysis.

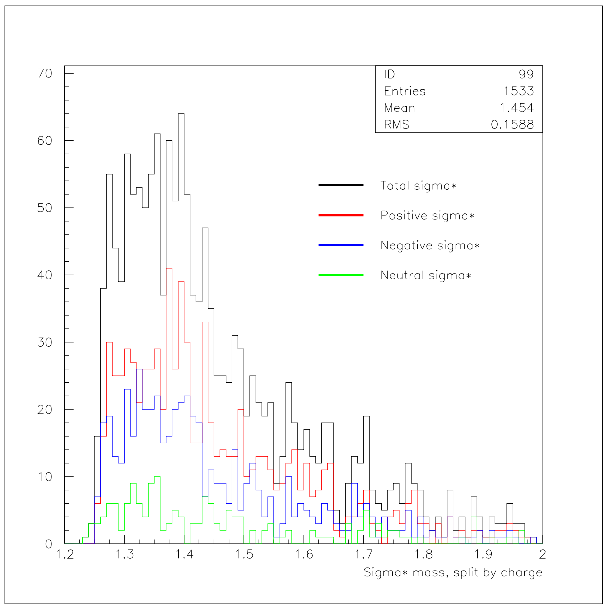

Figure 2.13: Invariant mass spectrum for Σ^* from 2000b1 data using the RICH for hadron identification. The red, blue, green, and black curves indicate positive, negative, neutral, and total Σ^*, respectively. It is almost impossible to identify a peak at the correct mass.

3 Developing spin-transfer models

3.1 Subprocess spin-transfer calculations

Given the observed agreement between the data and Monte Carlo on the reconstructed Σ^*/Λ yield ratio, it is reasonable to use the Monte Carlo to trace the origin of the Λ particles. The Λ production mechanisms may be classified in the following way:

- Current fragmentation with Λ produced directly from struck quark
- Current fragmentation with Λ produced as the decay product of another hyperon (Σ^*, Σ^0, Ξ^-, Ξ^0)[1] that contains the struck quark
- Hyperon (Λ, Σ^*, Σ^0, Ξ^-, Ξ^0) that does not contain the struck quark

Once these subprocess fractions are known, it is possible to construct a model of the total longitudinal spin-transfer coefficient $D_{LL'}^{\Lambda}$ as a function of z. The spin-transfer coefficient is a measure of the degree to which the polarization[2] of a Λ particle is influenced by the polarization of the struck quark:

$$P_q^{\Lambda} = P^{\mathrm{beam}} \cdot D(y)\; D_{LL'}^{\Lambda}.$$

This equation states that the polarization P_q^{Λ} of a Λ particle containing a struck quark q, is determined by the beam polarization P^{beam}, the photon depolarization factor $D(y)$, and $D_{LL'}^{\Lambda}$. The photon depolarization factor is a measure of the virtual photon polarization, given by the kinematics of the scattering process. This factor, in combination with the beam polarization, provides a measure of the struck quark polarization.

The spin-transfer coefficient can be calculated using the equation

$$D_{LL'}^{\Lambda} = \sum_q \sum_Y f_q^Y C_q^Y ,$$

where f_q^Y is the fractional contribution of a particular subprocess to Λ production, and C_q^Y is the amount of spin transfer in that subprocess. The subprocess fractions f_q^Y are obtained from the Monte Carlo. The individual spin-transfer coefficients C_q^Y must be calculated using one of several available models.

[1]There are very few Ξ^- and Ξ^0 particles produced at HERMES, and their contribution to Λ production is small.

[2]Polarization, in this case, is $\frac{M}{S}$, where M is the z-component of the spin and S is the total spin.

3.2 Elements of the spin-transfer coefficient C_q^Y

There are three questions that must be considered when calculating $C_q^Y = \langle P_q^\Lambda \rangle$:

- What happens to the spin of the struck quark during fragmentation?
- What is the probability $R_q^{M_Y}$ of producing a hyperon Y in spin state $|S_Y, M_Y\rangle$ from a polarized quark q?
- What is the probability $D_{M_Y \to M_\Lambda}$ for a hyperon Y in spin state $|S_Y, M_Y\rangle$ to decay into a Λ in spin state $|\frac{1}{2}, M_\Lambda\rangle$?

In the calculations presented here, we make two assumptions [12] about quarks in the fragmentation process. First, we assume perfect helicity conservation, i.e. the direction of the struck quark's spin (relative to its momentum vector) is preserved during fragmentation. Second, we assume that other quarks created during fragmentation have random polarizations. Thus, a hyperon that does not contain the struck quark has a random polarization, and $C_q^Y = 0$.

The production probability is defined as

$$R_q^{M_Y} = \frac{\langle \hat{n}_{q\uparrow} \rangle}{\sum_{M_Y} \langle \hat{n}_{q\uparrow} \rangle}, \tag{3.1}$$

where $\langle \hat{n}_{q\uparrow} \rangle$ is the expectation value of the number of spin-up quarks of flavor q in a particular hyperon Y. Calculation of $R_q^{M_Y}$ is model-dependent. Three different spin-structure models are presented in Sections 3.2.2 and 3.2.3. In contrast to $R_q^{M_Y}$, the decay probability $D_{M_Y \to M_\Lambda}$ is not model-dependent and can be calculated using simple angular momentum conservation arguments and Clebsch-Gordan coefficients (see Section 3.2.1).

In subprocesses where the Λ is produced as a decay product of a heavier hyperon, the Λ polarization is calculated using

$$\langle P_q^\Lambda \rangle = \sum_{M_Y} R_q^{M_Y} \sum_{M_\Lambda} D_{M_Y \to M_\Lambda} (\frac{M_\Lambda}{S_\Lambda}). \tag{3.2}$$

Figure 3.1 illustrates spin transfer from a polarized struck quark to a Λ with an intermediate Σ^* decay.

3.2.1 Calculation of decay probabilities $D_{M_Y \to M_\Lambda}$

As previously stated, the decay probability $D_{M_Y \to M_\Lambda}$ is not model-dependent and can be calculated from angular momentum conservation. As an example, we calculate $D_{M_{\Sigma^*} \to M_\Lambda}$, the probability for a Σ^* in spin state M_{Σ^*} to decay into a Λ in spin state M_Λ. The Σ^* is a spin-3/2 particle which decays to a Λ (spin-1/2) and π (spin-0). In order to conserve angular momentum, the final state must have orbital angular momentum $L = 1$. Therefore, for a Σ^* with a given M_{Σ^*}, we obtain

$$|\frac{3}{2}, M_{\Sigma^*}\rangle = |1, M_L\rangle \otimes |\frac{1}{2}, M_\Lambda\rangle.$$

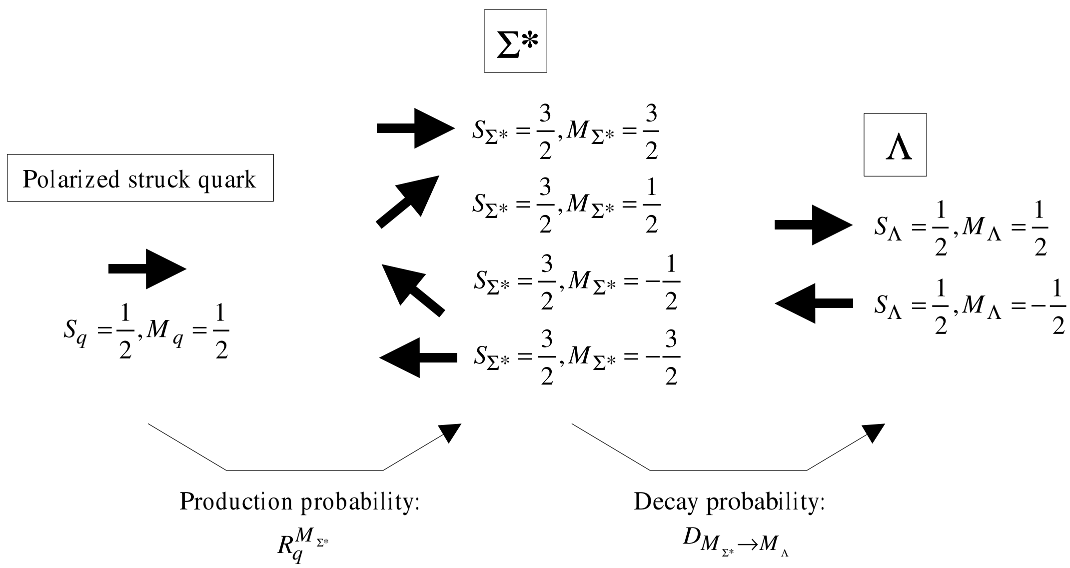

Figure 3.1: Spin-transfer schematic for a Λ produced from a Σ^* decay. A polarized quark with spin $|S_q, M_q\rangle = |\frac{1}{2}, \frac{1}{2}\rangle$ fragments into a Σ^* with spin $|S_{\Sigma^*}, M_{\Sigma^*}\rangle$; the production probability is $R_q^{M_{\Sigma^*}}$. The Σ^* then decays, with probability $D_{M_{\Sigma^*} \to M_\Lambda}$, into a Λ with spin $|S_\Lambda, M_\Lambda\rangle$.

Note that there is no contribution from the π since it is a spin-0 particle. Using the Clebsch-Gordan coefficients to express $|\frac{3}{2}, M_{\Sigma^*}\rangle$ in terms of $|1, M_L\rangle$ and $|\frac{1}{2}, M_\Lambda\rangle$, it is possible to determine the probability of the Λ particle having $M_\Lambda = \frac{1}{2}$ or $M_\Lambda = -\frac{1}{2}$ (see Table 3.1).

Table 3.1: Probability of Λ carrying $M_\Lambda = \frac{1}{2}$ or $-\frac{1}{2}$ given a particular M_{Σ^*}

$\lvert\frac{3}{2}, M_{\Sigma^*}\rangle$	$\lvert M_L, M_\Lambda\rangle$	$D_{M_{\Sigma^*} \to \frac{1}{2}}$	$D_{M_{\Sigma^*} \to -\frac{1}{2}}$
$\lvert\frac{3}{2}, \frac{3}{2}\rangle$	$\lvert 1, \frac{1}{2}\rangle$	1	0
$\lvert\frac{3}{2}, \frac{1}{2}\rangle$	$\sqrt{\frac{1}{3}}\lvert 1, -\frac{1}{2}\rangle + \sqrt{\frac{2}{3}}\lvert 0, \frac{1}{2}\rangle$	$\frac{2}{3}$	$\frac{1}{3}$
$\lvert\frac{3}{2}, -\frac{1}{2}\rangle$	$\sqrt{\frac{2}{3}}\lvert 0, -\frac{1}{2}\rangle + \sqrt{\frac{1}{3}}\lvert -1, \frac{1}{2}\rangle$	$\frac{1}{3}$	$\frac{2}{3}$
$\lvert\frac{3}{2}, -\frac{3}{2}\rangle$	$\lvert -1, -\frac{1}{2}\rangle$	0	1

Using Equation 3.2 and the values of $D_{M_{\Sigma^*} \to M_\Lambda}$ given by Table 3.1, we can write $\langle P_q^\Lambda \rangle$ in terms of the production probabilities $R_q^{M_{\Sigma^*}}$:

$$\begin{aligned}
\langle P_q^\Lambda \rangle &= R_q^{M_{\frac{3}{2}}}(1-0) + R_q^{M_{\frac{1}{2}}}(\frac{2}{3} - \frac{1}{3}) + R_q^{M_{-\frac{1}{2}}}(\frac{1}{3} - \frac{2}{3}) + R_q^{M_{-\frac{3}{2}}}(0-1) \\
&= R_q^{M_{\frac{3}{2}}} + \frac{1}{3}R_q^{M_{\frac{1}{2}}} - \frac{1}{3}R_q^{M_{-\frac{1}{2}}} - R_q^{M_{-\frac{3}{2}}}.
\end{aligned}$$

Similarly,

$$\begin{aligned}\langle P_q^{\Sigma^*}\rangle &= \sum_{M_{\Sigma^*}} R_q^{M_{\Sigma^*}}(\frac{M_{\Sigma^*}}{S_{\Sigma^*}}) \\ &= \frac{\frac{3}{2}R_q^{M_{\frac{3}{2}}} + \frac{1}{2}R_q^{M_{\frac{1}{2}}} - \frac{1}{2}R_q^{M_{-\frac{1}{2}}} - \frac{3}{2}R_q^{M_{-\frac{3}{2}}}}{\frac{3}{2}} \\ &= R_q^{M_{\frac{3}{2}}} + \frac{1}{3}R_q^{M_{\frac{1}{2}}} - \frac{1}{3}R_q^{M_{-\frac{1}{2}}} - R_q^{M_{-\frac{3}{2}}} \\ &= \langle P_q^{\Lambda}\rangle.\end{aligned}$$

The above calculations show that $\langle P_q^{\Lambda}\rangle = \langle P_q^{\Sigma^*}\rangle$ throughout the decay of the Σ^*. The relationships between $\langle P_q^{\Lambda}\rangle$ and the polarizations of other hyperon parents (Σ^0, Ξ^-, Ξ^0) are listed in Table 3.2; the calculations are described in Appendix A.

Table 3.2: Relationship of $\langle P_q^{\Lambda}\rangle$ to parent polarization

	Σ^*	Σ^0	Ξ^0	Ξ^-
$\langle P_q^{\Lambda}\rangle$	$\langle P_q^{\Sigma^*}\rangle$	$-\frac{1}{3}\langle P_q^{\Sigma^0}\rangle$	$\langle P_q^{\Xi^0}\rangle$	$\langle P_q^{\Xi^-}\rangle$

3.2.2 Hyperon spin structure 1: Naïve constituent quark model

It is possible to calculate C_q^Y using the naïve constituent quark model, which assumes that a baryon is composed of three non-interacting quarks with zero orbital angular momentum, and that the spin of the baryon comes entirely from the quarks.

We begin by calculating the average polarization of a Λ particle produced directly from the struck quark. In this subprocess, it is necessary to consider only $R_q^{M_\Lambda}$ since there is no intermediate hyperon decay ($D_{M_Y \to M_\Lambda} = 1$). To calculate $R_q^{M_\Lambda}$, we start by constructing the spin–flavor wavefunction of the Λ for $M_\Lambda = \frac{1}{2}$ and $M_\Lambda = -\frac{1}{2}$. Because quarks are fermions, the total wavefunction (flavor + spin + spatial + color) of the Λ must be antisymmetric. All baryons are color singlets, i.e. the color component of the wavefunctions is antisymmetric, and ground-state wavefunctions have zero angular momentum, so the spatial component is symmetric. The combination of the remaining two components, flavor and spin, must therefore be symmetric. The Λ is a member of the baryon octet with mixed flavor symmetry; its spin–flavor wavefunctions $|\frac{1}{2}, M_\Lambda\rangle$ are

$$\begin{aligned}|\frac{1}{2},\frac{1}{2}\rangle = \frac{1}{\sqrt{12}}(&u^\uparrow d^\downarrow s^\uparrow - u^\downarrow d^\uparrow s^\uparrow - d^\uparrow u^\downarrow s^\uparrow + d^\downarrow u^\uparrow s^\uparrow + d^\downarrow s^\uparrow u^\uparrow - d^\uparrow s^\uparrow u^\downarrow \\ &-u^\downarrow s^\uparrow d^\uparrow + u^\uparrow s^\uparrow d^\downarrow + s^\uparrow u^\uparrow d^\downarrow - s^\uparrow u^\downarrow d^\uparrow - s^\uparrow d^\uparrow u^\downarrow + s^\uparrow d^\downarrow u^\uparrow),\end{aligned}$$

Table 3.3: Expectation values of the number of spin-up u, d, and s quarks in Λ

Lambda spin state	$\langle \hat{n}_{u\uparrow} \rangle$	$\langle \hat{n}_{d\uparrow} \rangle$	$\langle \hat{n}_{s\uparrow} \rangle$
$\vert\frac{1}{2}, \frac{1}{2}\rangle$	$\frac{1}{2}$	$\frac{1}{2}$	1
$\vert\frac{1}{2}, -\frac{1}{2}\rangle$	$\frac{1}{2}$	$\frac{1}{2}$	0

$$\begin{aligned}|\frac{1}{2}, -\frac{1}{2}\rangle = \frac{1}{\sqrt{12}}(&s^{\downarrow}u^{\uparrow}d^{\downarrow} - s^{\downarrow}d^{\uparrow}u^{\downarrow} + d^{\downarrow}u^{\uparrow}s^{\downarrow} - u^{\downarrow}d^{\uparrow}s^{\downarrow} + u^{\uparrow}s^{\downarrow}d^{\downarrow} - d^{\uparrow}s^{\downarrow}u^{\downarrow} \\ &+u^{\uparrow}d^{\downarrow}s^{\downarrow} - d^{\uparrow}u^{\downarrow}s^{\downarrow} + s^{\downarrow}d^{\downarrow}u^{\uparrow} - s^{\downarrow}u^{\downarrow}d^{\uparrow} + d^{\downarrow}s^{\downarrow}u^{\uparrow} - u^{\downarrow}s^{\downarrow}d^{\uparrow}).\end{aligned}$$

(Detailed methods for constructing spin–flavor wavefunctions for the baryon octet can be found in reference [5].) Table 3.3 lists the values of $\langle \hat{n}_{q\uparrow} \rangle$ calculated from these Λ wavefunctions. We use these expectation values and Equations 3.1, 3.2 to calculate the ensemble average of the polarization of the Λ:

$$\begin{aligned}\langle P_u^{\Lambda} \rangle &= \frac{\sum_{M_\Lambda} \langle \hat{n}_{u\uparrow} \rangle (\frac{M_\Lambda}{S_\Lambda})}{\sum_{M_\Lambda} \langle \hat{n}_{u\uparrow} \rangle} \\ &= \frac{\frac{1}{2}(1) + \frac{1}{2}(-1)}{\frac{1}{2} + \frac{1}{2}} \\ &= 0 \\ \langle P_d^{\Lambda} \rangle &= \frac{\sum_{M_\Lambda} \langle \hat{n}_{u\uparrow} \rangle (\frac{M_\Lambda}{S_\Lambda})}{\sum_{M_\Lambda} \langle \hat{n}_{d\uparrow} \rangle} \\ &= \frac{\frac{1}{2}(1) + \frac{1}{2}(-1)}{\frac{1}{2} + \frac{1}{2}} \\ &= 0 \\ \langle P_s^{\Lambda} \rangle &= \frac{\sum_{M_\Lambda} \langle \hat{n}_{u\uparrow} \rangle (\frac{M_\Lambda}{S_\Lambda})}{\sum_{M_\Lambda} \langle \hat{n}_{s\uparrow} \rangle} \\ &= \frac{1(1) + 0(-1)}{1 + 0} \\ &= 1.\end{aligned}$$

These polarization values are equal to the spin-transfer coefficients for the subprocess in which a Λ is produced directly from the struck quark. The values indicate that the Λ polarization is not influenced by a struck up or down quark; however, the spin of the Λ is determined entirely by a struck strange quark.

As a second example, we calculate the average polarization of a Λ produced from a positive Σ^* containing the struck quark, beginning with the production probability $R_q^{M_{\Sigma^*}}$. We start by constructing the spin–flavor wavefunction of the Σ^*. For a positive Σ^* (quark

Table 3.4: Expectation values of the number of spin-up u and s quarks in positive Σ^*

Positive Σ^* spin–flavor wavefunction	$\langle \hat{n}_{u\uparrow} \rangle$	$\langle \hat{n}_{s\uparrow} \rangle$
$\lvert\frac{3}{2}, \frac{3}{2}\rangle = (u^\uparrow u^\uparrow s^\uparrow)$	2	1
$\lvert\frac{3}{2}, \frac{1}{2}\rangle = \sqrt{\frac{1}{3}}(u^\uparrow u^\uparrow s^\downarrow + u^\uparrow u^\downarrow s^\uparrow + u^\downarrow u^\uparrow s^\uparrow)$	$\frac{4}{3}$	$\frac{2}{3}$
$\lvert\frac{3}{2}, -\frac{1}{2}\rangle = \sqrt{\frac{1}{3}}(u^\uparrow u^\downarrow s^\downarrow + u^\downarrow u^\uparrow s^\downarrow + u^\downarrow u^\downarrow s^\uparrow)$	$\frac{2}{3}$	$\frac{1}{3}$
$\lvert\frac{3}{2}, -\frac{3}{2}\rangle = (u^\downarrow u^\downarrow s^\downarrow)$	0	0

content = uus), we obtain the following combinations of spin and flavor for different $|\frac{3}{2}, M_{\Sigma^*}\rangle$ (ignoring normalization constants):

$$
\begin{aligned}
|\frac{3}{2}, \frac{3}{2}\rangle &= (uus + usu + suu) \otimes (\uparrow\uparrow\uparrow) \\
|\frac{3}{2}, \frac{1}{2}\rangle &= (uus + usu + suu) \otimes (\downarrow\uparrow\uparrow + \uparrow\downarrow\uparrow + \uparrow\uparrow\downarrow) \\
|\frac{3}{2}, -\frac{1}{2}\rangle &= (uus + usu + suu) \otimes (\downarrow\downarrow\uparrow + \uparrow\downarrow\downarrow + \downarrow\uparrow\downarrow) \\
|\frac{3}{2}, -\frac{3}{2}\rangle &= (uus + usu + suu) \otimes (\downarrow\downarrow\downarrow).
\end{aligned}
$$

Note that the Σ^*, unlike the Λ, is a member of the spin-3/2 baryon decuplet and has symmetric flavor and spin wavefunction components. Re-writing and normalizing the spin–flavor wavefunctions, we calculate the expectation values of the number of spin-up u and s quarks in a positive Σ^* (see Table 3.4).

Using Equation 3.1 and the values of $\langle \hat{n}_{q\uparrow} \rangle$ given in Table 3.4, we calculate the ensemble average of the polarization of the positive Σ^*:

$$
\begin{aligned}
\langle P_u^{\Sigma^*} \rangle &= \sum_{M_{\Sigma^*}} R_u^{M_{\Sigma^*}} (\frac{M_{\Sigma^*}}{S_{\Sigma^*}}) \\
&= \frac{\sum_{M_{\Sigma^*}} \langle \hat{n}_{u\uparrow} \rangle (\frac{M_{\Sigma^*}}{S_{\Sigma^*}})}{\sum_{M_{\Sigma^*}} \langle \hat{n}_{u\uparrow} \rangle} \\
&= \frac{2(1) + \frac{4}{3}(\frac{1}{3}) - \frac{2}{3}(\frac{1}{3}) - 0}{2 + \frac{4}{3} + \frac{2}{3}} \\
&= \frac{5}{9} \\
\langle P_s^{\Sigma^*} \rangle &= \sum_{M_{\Sigma^*}} R_s^{M_{\Sigma^*}} (\frac{M_{\Sigma^*}}{S_{\Sigma^*}}) \\
&= \frac{\sum_{M_{\Sigma^*}} \langle \hat{n}_{s\uparrow} \rangle (\frac{M_{\Sigma^*}}{S_{\Sigma^*}})}{\sum_{M_{\Sigma^*}} \langle \hat{n}_{s\uparrow} \rangle}
\end{aligned}
$$

$$= \frac{1(1) + \frac{2}{3}(\frac{1}{3}) - \frac{1}{3}(\frac{1}{3}) - 0}{1 + \frac{2}{3} + \frac{1}{3}}$$

$$= \frac{5}{9}.$$

As described in Table 3.2, $\langle P_q^\Lambda \rangle = \langle P_q^{\Sigma^*} \rangle$. We thus obtain the final spin–transfer coefficients for Λ from positive Σ^*: $\langle P_u^\Lambda \rangle = \frac{5}{9}$ and $\langle P_s^\Lambda \rangle = \frac{5}{9}$. Similarly, $\langle P_d^\Lambda \rangle = \langle P_s^\Lambda \rangle = \frac{5}{9}$ for negative Σ^* (quark content = dds), and $\langle P_u^\Lambda \rangle = \langle P_d^\Lambda \rangle = \langle P_s^\Lambda \rangle = \frac{5}{9}$ for neutral Σ^* (quark content = uds). Subprocess spin–transfer calculations for Λ particles produced from Σ^0, Ξ^-, and Ξ^0 are described in Appendix A. Table 3.5 lists the individual spin–transfer coefficients C_q^Y for hyperons either containing the struck quark (u, d, or s) or not containing the struck quark (n).

Table 3.5: Subprocess spin-transfer coefficients C_q^Y in the naïve constituent quark model

	u	d	s	n
Λ	0	0	1	0
Positive Σ^*	$\frac{5}{9}$	0	$\frac{5}{9}$	0
Neutral Σ^*	$\frac{5}{9}$	$\frac{5}{9}$	$\frac{5}{9}$	0
Negative Σ^*	0	$\frac{5}{9}$	$\frac{5}{9}$	0
Σ^0	$-\frac{2}{9}$	$-\frac{2}{9}$	$\frac{1}{9}$	0
Ξ^0	$-\frac{1}{3}$	0	$\frac{2}{3}$	0
Ξ^-	0	$-\frac{1}{3}$	$\frac{2}{3}$	0

3.2.3 Hyperon spin structure 2: SU(3) symmetric models

A more sophisticated method of calculating the spin-transfer coefficients C_q^Y is to use SU(3) symmetry to relate the proton spin structure, which is well known, to the spin structure of other members of the baryon octet [8]. To perform this calculation, recall that the first moments of the parton distribution functions are defined as $\Delta q \equiv \langle \hat{n}_{q\uparrow} \rangle - \langle \hat{n}_{q\downarrow} \rangle$ and $q \equiv \langle \hat{n}_{q\uparrow} \rangle + \langle \hat{n}_{q\downarrow} \rangle$. In a hyperon Y, we express $\langle \hat{n}_{q\uparrow} \rangle$ for the two extreme M_Y states in terms of q_Y and Δq_Y:

$$\langle \hat{n}_{q\uparrow} \rangle_{M_Y = S_Y} = \frac{q_Y + \Delta q_Y}{2}$$

$$\langle \hat{n}_{q\uparrow} \rangle_{M_Y = -S_Y} = \langle \hat{n}_{q\downarrow} \rangle_{M_Y = S_Y} = \frac{q_Y - \Delta q_Y}{2}.$$

Table 3.6: Subprocess spin-transfer coefficients C_q^Y calculated using the Burkardt–Jaffe SU(3) symmetric model

	u	d	s	n
Λ	-0.17	-0.17	0.63	0
Positive Σ^*	0.38	0	0.55	0
Neutral Σ^*	0.38	0.38	0.55	0
Negative Σ^*	0	0.38	0.55	0
Σ^0	-0.12	-0.12	0.14	0
Ξ^0	-0.43	-0.10	0.42	0
Ξ^-	-0.10	-0.43	0.42	0

Expressions for the intermediate M_Y states are obtained using

$$\langle \hat{n}_{q\uparrow} \rangle_{M_Y} = \frac{q_Y}{2} + (\frac{M_Y}{S_Y})\frac{\Delta q_Y}{2},$$

a linear interpolation between the two extreme values. The polarization of a hyperon Y produced from a struck quark q, expressed in terms of Δq_Y and q_Y, is

$$\begin{aligned}
\langle P_q^Y \rangle &= \sum_{M_Y} R_q^{M_Y} (\frac{M_Y}{S_Y}) \\
&= \frac{\sum_{M_Y} \langle \hat{n}_{q\uparrow} \rangle (\frac{M_Y}{S_Y})}{\sum_{M_Y} \langle \hat{n}_{q\uparrow} \rangle} \\
&= \frac{\sum_{M_Y} [\frac{q_Y}{2} + (\frac{M_Y}{S_Y})\frac{\Delta q_Y}{2}](\frac{M_Y}{S_Y})}{\sum_{M_Y} [\frac{q_y}{2} + (\frac{M_Y}{S_Y})\frac{\Delta q_Y}{2}]} \\
&= \frac{\Delta q_Y}{q_Y}(\frac{1}{2S_Y+1}) \sum_{M_Y} (\frac{M_Y}{S_Y})^2,
\end{aligned}$$

where we have used the fact that $\sum_{M_Y} M_Y = 0$. The polarizations of spin-1/2 and spin-3/2 baryons are therefore

- Spin-1/2 baryon: $\langle P_q^Y \rangle = \frac{\Delta q_Y}{q_Y}$
- Spin-3/2 baryon: $\langle P_q^Y \rangle = \frac{5}{9}(\frac{\Delta q_Y}{q_Y})$.

The procedure for obtaining values of Δq and q in the Burkardt–Jaffe SU(3) symmetric model is outlined in references [5, 8]. Using the values of $\Delta Q = \Delta q + \Delta \bar{q}$ given in reference [15] and hyperon decay probabilities given in Table 3.2, we obtain C_q^Y in the Burkardt–Jaffe SU(3) symmetric model (Table 3.6).

Table 3.7: Subprocess spin-transfer coefficients C_q^Y calculated using the Ashery–Lipkin SU(3) valence model

	u	d	s	n
Λ	-0.07	-0.07	0.73	0
Positive Σ^*	0.38	0	0.55	0
Neutral Σ^*	0.38	0.38	0.55	0
Negative Σ^*	0	0.38	0.55	0
Σ^0	-0.16	-0.16	0.11	0
Ξ^0	-0.33	0.00	0.47	0
Ξ^-	0.00	-0.33	0.47	0

The Burkardt–Jaffe SU(3) symmetric model is modified by Ashery and Lipkin in reference [15] so that valence quarks and sea quarks contribute separately to ΔQ. The contribution ΔQ_s from the sea quarks is subtracted from the total ΔQ, leaving behind Δq for the valence quarks. Only the values of Δq for the valence quarks are used for calculating the polarization of Λ particles produced in fragmentation. The spin-transfer coefficients C_q^Y in the Ashery–Lipkin SU(3) valence model are listed in Table 3.7.

The values of $\Delta q/q$ for Ξ^0 and Ξ^- are not explicitly given in reference [15]. We assume that the Ξ^0 (quark content uss) can be related to the proton (quark content uud) in the following manner:

$$\frac{\Delta u_p}{u_p} = \frac{\Delta s_{\Xi^0}}{s_{\Xi^0}}$$
$$\frac{\Delta d_p}{d_p} = \frac{\Delta u_{\Xi^0}}{u_{\Xi^0}}.$$

Similarly, Ξ^- (quark content dss) has

$$\frac{\Delta u_p}{u_p} = \frac{\Delta s_{\Xi^-}}{s_{\Xi^-}}$$
$$\frac{\Delta d_p}{d_p} = \frac{\Delta d_{\Xi^-}}{d_{\Xi^-}}.$$

It should also be noted that Σ^* is not a member of the baryon octet; therefore, the Σ^* spin structure cannot be derived from the proton spin structure through an SU(3) rotation. To obtain values of $\Delta q_{\Sigma^*}/q_{\Sigma^*}$, we assume that the ratio of $\Delta q_{\Sigma^*}/q_{\Sigma^*}$ to $\Delta q_{\Sigma^0}/q_{\Sigma^0}$ is the same in the SU(3) and naïve constituent quark models [15]. In the naïve constituent quark model $\Delta u_{\Sigma^0}/u_{\Sigma^0} = \Delta d_{\Sigma^0}/d_{\Sigma^0} = 2/3$ and $\Delta s_{\Sigma^0}/s_{\Sigma^0} = -1/3$; $\Delta u_{\Sigma^*}/u_{\Sigma^*} = \Delta d_{\Sigma^*}/d_{\Sigma^*} = \Delta s_{\Sigma^*}/s_{\Sigma^*} = 1/3$. The ratios of $\Delta q_{\Sigma^*}/q_{\Sigma^*}$ to $\Delta q_{\Sigma^0}/q_{\Sigma^0}$ are therefore $1/2$, $1/2$, and -1 for

$\Delta u/u$, $\Delta d/d$, and $\Delta s/s$, respectively. Given $\Delta u_{\Sigma^0}/u_{\Sigma^0} = \Delta d_{\Sigma^0}/d_{\Sigma^0} = 0.47$ and $\Delta s_{\Sigma^0}/s_{\Sigma^0} = -0.33$, we obtain $\Delta u_{\Sigma^*}/u_{\Sigma^*} = \Delta d_{\Sigma^*}/d_{\Sigma^*} = 0.23$ and $\Delta s_{\Sigma^*}/s_{\Sigma^*} = 0.33$.[3]

[3]Ashery and Lipkin use the convention $\Delta u + \Delta d + \Delta s = 1$ (instead of $\Delta u + \Delta d + \Delta s = 3$) for Σ^*. To correct for this, $\langle P_q^{\Sigma^*}\rangle$ must be multiplied by an additional factor of three.

4 Results and discussion

4.1 Tracing the origin of Λ particles

A total of 180000 Monte Carlo events containing "real" Λ particles were used to determine production mechanisms (63 million generated events). Each event was required to have at least two tracks in addition to the scattered positron—a proton and negatively-charged pion from a Λ that were within the acceptance of the HERMES spectrometer and had momentum greater than 0.2 GeV$/c^2$. Subprocess fractions for Λ production as a function of z were calculated by identifying the struck quark and the direct parent of Λ particles in generated events (a detailed description of this procedure is given in Appendix B).

Figure 4.1 shows the fractions of Λ particles as a function of z grouped by parent: direct Λ production from string fragmentation, and Λ particles resulting from the decay of Σ^0, Σ^*, and Ξ. The subprocesses considered in Figure 4.1 can be further subdivided by the flavor of the struck quark. The hyperon produced directly in an event (Λ, Σ^*, Σ^0, Ξ) may contain an up, down, or strange struck quark, or may not contain the struck quark at all. Figure 4.2 shows the fractions of hyperons containing various flavors of the struck quark as a function of z. On average, only about 10% of the Λ particles produced at HERMES come from the struck quark; at high values of z, the fraction increases to about 50%. When Λ particles contain the struck quark, scattering from up quarks is dominant for values of z up to about 0.7. Up quark dominance is to be expected, since the semi-inclusive DIS cross section is proportional to the square of the charge of the struck quark. The up quark, with a charge of $\frac{2}{3}$, is therefore four times as likely to be struck as a down or strange quark, both with charge $-\frac{1}{3}$. At higher values of z, scattering from up quarks becomes suppressed, and scattering from strange quarks becomes enhanced. This result is somewhat surprising but can likely be explained by the fact that at high z, there is more available energy for the creation of strange quarks.

Using the subprocess fraction and struck quark information, it is possible to calculate the overall longitudinal spin transfer coefficient $D^{\Lambda}_{LL'} = \sum_q \sum_Y f^Y_q C^Y_q$. The fractional contributions f^Y_q of particular subprocesses to Λ production are obtained from the above Monte Carlo results. The individual spin transfer coefficients C^Y_q are calculated using the naïve constituent quark model, the Burkardt–Jaffe SU(3) symmetric model, or the Ashery–Lipkin SU(3) valence model, together with the previously described assumptions about quark helicity in the fragmentation process. We thus obtain three Monte Carlo predictions for $D^{\Lambda}_{LL'}$ as a function of z; these are shown in Figure 4.3 along with various other model predictions and actual HERMES data.

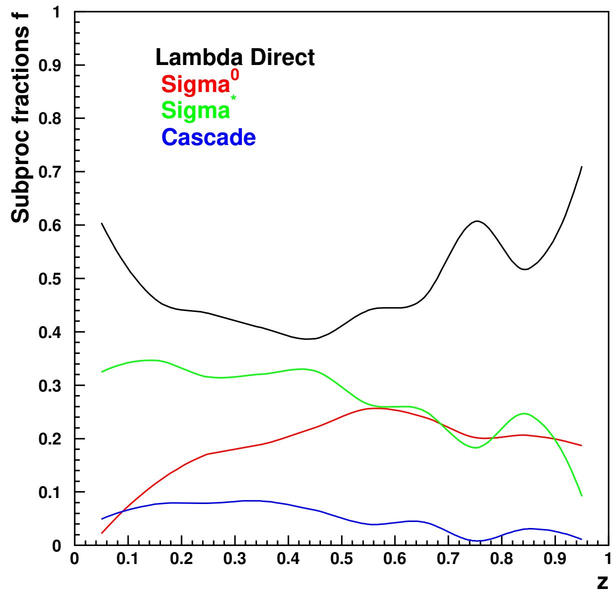

Figure 4.1: Fractions of Λ particles originating from various sources as a function of z. The black curve shows the fraction of Λ particles produced directly from the target (struck quark, target remnant, or other process). The red, green, and blue curves show the fraction of Λ particles produced as decay products of Σ^0, Σ^*, and Ξ, respectively.

4.2 Hyperon yields in data, Monte Carlo

We have found that Σ^* particles are visible in the data; however, the statistics are extremely low. The data and Monte Carlo agree very well on the Σ^*/Λ yield ratio, but disagree on the signal-to-background ratio and width of the Λ mass spectrum itself. Further tuning of the Monte Carlo parameters is needed in order to bring the Λ yield into agreement with the data.

4.3 Lambda production mechanisms

The main result of this analysis is that the majority of Λ particles produced at HERMES ($\geq 90\%$) do not contain the struck quark. The few Λ particles that are produced in the current fragmentation region contain mostly struck u quarks ($z < 0.7$); s quark dominance does not appear until $z > 0.8$. We have also found that about 40%-60% of Λ particles are produced from heavier hyperons, depending on the value of z. Because so few Λ particles contain the struck quark (and even fewer contain struck s quarks), it is not surprising that the observed $D^{\Lambda}_{LL'}$ is so small at HERMES. One consequence of this result is that it is not feasible to use Λ particles as spin probes for accessing structure functions that are currently of interest, such as transversity.

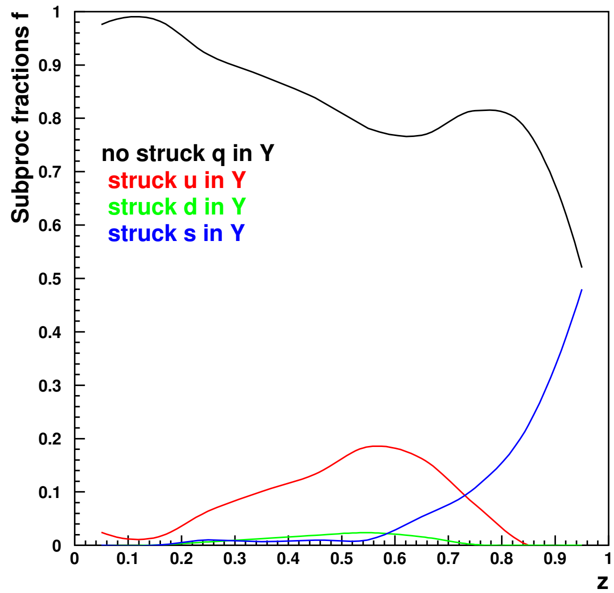

Figure 4.2: Fractions of hyperons (Λ, Σ^*, Σ^0, Ξ) containing different flavors of the struck quark as a function of z. The black curve shows the fraction of hyperons produced that do not contain the struck quark. The red, green, and blue curves show the fraction of hyperons produced that contain up, down, and strange struck quarks, respectively.

4.4 Monte Carlo models for $D^{\Lambda}_{LL'}$

The models for $D^{\Lambda}_{LL'}$ that we have constructed using Monte Carlo subprocess fractions and simple calculations for C^Y_q indicate that $D^{\Lambda}_{LL'}$ is small and rises to about 40% at the highest values of z. The different methods used to calculate C^Y_q (naïve constituent quark model, Burkardt–Jaffe SU(3) symmetric model, and Ashery–Lipkin SU(3) valence model) produce very similar predictions for $D^{\Lambda}_{LL'}$. We therefore conclude that $D^{\Lambda}_{LL'}$ is sensitive primarily to the subprocess fractions f^Y_q and that we cannot use HERMES spin-transfer data to determine which model most accurately describes hyperon spin structure. In contrast to HERMES, ALEPH [10] and OPAL [11] have previously observed a significant degree of spin transfer to Λ particles. We can reconcile these differences by noting that both ALEPH and OPAL are colliding beam experiments at a higher kinematic range than HERMES, which is a fixed target experiment. At HERMES energies, it is very difficult to form a Λ from the struck quark—it is necessary for multiple quarks or a diquark to be produced in the fragmentation process. It is much easier to form a Λ from the target remnant because, for example, in the case of a struck u quark, only one $s\bar{s}$ pair needs to be created during fragmentation.

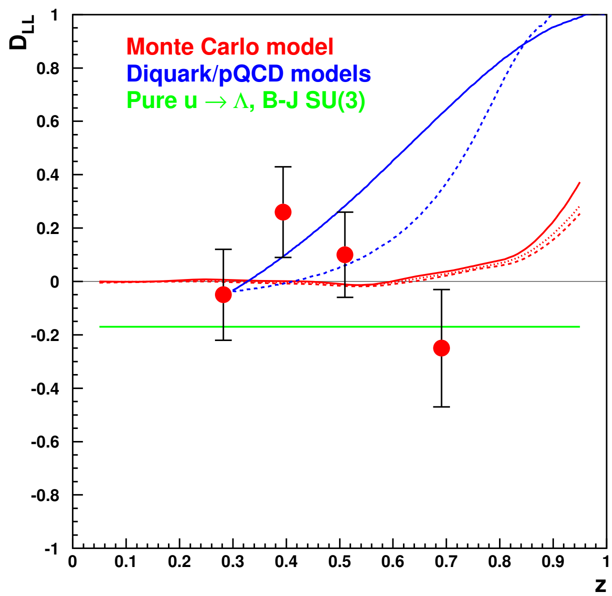

Figure 4.3: Monte Carlo predictions for $D^{\Lambda}_{LL'}$ as a function of z (indicated by the red curves)—the solid, dashed, and dotted lines indicate the naïve quark model, Burkardt–Jaffe SU(3) symmetric model, and Ashery–Lipkin SU(3) valence model, respectively. Also shown are curves predicted from quark–diquark and perturbative QCD models [13]. HERMES spin transfer data points are superimposed for comparison.

4.5 Future work

As stated above, one of the most important issues to address at this point is the discrepancy between the Λ yield in the data and in the Monte Carlo, since it is uncertain how this disagreement affects the results presented in this thesis. It is also necessary to perform a more thorough comparison of the Σ^0/Λ yield ratio, as another test of the accuracy of the Monte Carlo.

The Monte Carlo models for $D^{\Lambda}_{LL'}$ developed here are successful in that they predict essentially zero spin transfer to Λ particles up to about $z = 0.7$; this is qualitatively consistent with the data. However, the shape of the data is rather poorly matched by the Monte Carlo, suggesting that our current spin-transfer models are too simple. Since the Monte Carlo indicates that many of the Λ particles observed at HERMES are produced in the target fragmentation region, it may be of interest to reconsider the polarization of Λ particles containing the target remnant, instead of assuming that the polarization is simply zero. This study primarily provides a rough explanation for the HERMES spin-transfer data; with more sophisticated models and modified Monte Carlo parameters, it may be possible to achieve a more detailed understanding in the future.

Bibliography

[1] EMC Collaboration, J. Ashman et al., Nucl. Phys. **B328** (1989) 1.

[2] SMC Collaboration, B. Adeva et al., Phys. Lett. B **420** (1998) 180.

[3] HERMES Collaboration, K. Ackerstaff et al., Phys. Lett. B **464** (1999) 123.

[4] J. I. Friedman and H. W. Kendall, Ann. Rev. Nucl. Sci. **22** (1972) 203.

[5] G. Schnell, Ph.D. Thesis, New Mexico State University, May 1999 (unpublished, available at **http://hermes.desy.de/notes**).

[6] A.A. Sokolov and I.M. Ternov, Sov. Phys. Doklady **8** (1964) 1203.

[7] HERMES Collaboration, K. Ackerstaff et al., Nucl. Instrum. Methods A **417** (1998) 230.

[8] M. Burkardt and R. L. Jaffe, Phys. Rev. Lett. **70** (1993) 2537.

[9] R. L. Jaffe, Phys. Rev. D **54**, (1996) R6581; and references therein.

[10] ALEPH Collaboration, D. Buskulic et al., Phys. Lett. B **374** (1996) 319.

[11] OPAL Collaboration, K. Ackerstaff et al., Eur. Phys. J. C **2** (1998) 49.

[12] G. Gustafson and J. Häkkinen, Phys. Lett. B **303** (1993) 350.

[13] B.-Q. Ma, I. Schmidt and J.-J. Yang, Phys. Rev. D **61** (2000) 034017.

[14] B.-Q. Ma, I. Schmidt, J. Soffer, and J.-J. Yang, Phys. Rev. D **65** (2002) 034004.

[15] D. Ashery and H. J. Lipkin, Phys. Lett. B **469** (1999) 263.

A Spin-transfer derivations

Complete derivations for the subprocess spin-transfer coefficients $C_q^{\prime Y}$ in the naïve quark model are described in this appendix. The subprocesses listed include Λ particles produced from Σ^0, Ξ^0, and Ξ^- parents that contain the struck quark.

A.1 Lambda produced from Σ^0

The Σ^0 is a spin-1/2 particle with quark content = uds that decays to a Λ (spin-1/2) and photon (spin-1). We begin by calculating the decay probability $D_{M_{\Sigma^0} \to M_\Lambda}$. Writing the angular momenta of the decay products in terms of the angular momentum of the parent Σ^0, we obtain

$$|\frac{1}{2}, M_{\Sigma^0}\rangle = |1, M_\gamma\rangle \otimes |\frac{1}{2}, M_\Lambda\rangle.$$

Using the Clebsch-Gordan coefficients, it is possible to determine the probability of the Λ particle having $M_\Lambda = \frac{1}{2}$ or $M_\Lambda = -\frac{1}{2}$ (see Table A.1).

Writing $\langle P_q^\Lambda \rangle$ and $\langle P_q^{\Sigma^0} \rangle$ in terms of the production probabilities $R_q^{M_{\Sigma^0}}$, we obtain the following:

$$\begin{aligned}
\langle P_q^\Lambda \rangle &= R_q^{M_{\frac{1}{2}}}(\frac{1}{3} - \frac{2}{3}) + R_q^{M_{-\frac{1}{2}}}(\frac{2}{3} - \frac{1}{3}) \\
&= -\frac{1}{3} R_q^{M_{\frac{1}{2}}} + \frac{1}{3} R_q^{M_{-\frac{1}{2}}} \\
\langle P_q^{\Sigma^0} \rangle &= \frac{\frac{1}{2} R_q^{M_{\frac{1}{2}}} - \frac{1}{2} R_q^{M_{-\frac{1}{2}}}}{\frac{1}{2}} \\
&= R_q^{M_{\frac{1}{2}}} - R_q^{M_{-\frac{1}{2}}} \\
&= -3 \langle P_q^\Lambda \rangle
\end{aligned} \tag{A.1}$$

Table A.1: Probability of Λ carrying $M_\Lambda = \frac{1}{2}$ or $-\frac{1}{2}$ given a particular M_{Σ^0}

$\lvert\frac{1}{2}, M_{\Sigma^0}\rangle$	$\lvert M_\gamma, M_\Lambda\rangle$	$D_{M_{\Sigma 0}\to\frac{1}{2}}$	$D_{M_{\Sigma 0}\to-\frac{1}{2}}$
$\lvert\frac{1}{2}, \frac{1}{2}\rangle$	$\sqrt{\frac{2}{3}}\lvert 1, -\frac{1}{2}\rangle - \sqrt{\frac{1}{3}}\lvert 0, \frac{1}{2}\rangle$	$\frac{1}{3}$	$\frac{2}{3}$
$\lvert\frac{1}{2}, -\frac{1}{2}\rangle$	$\sqrt{\frac{1}{3}}\lvert 0, -\frac{1}{2}\rangle - \sqrt{\frac{2}{3}}\lvert -1, \frac{1}{2}\rangle$	$\frac{2}{3}$	$\frac{1}{3}$

Table A.2: Expectation values of the number of spin-up up, down, and strange quarks in Σ^0

Σ^0 spin–flavor wavefunction	$\langle\hat{n}_{u\uparrow}\rangle$	$\langle\hat{n}_{d\uparrow}\rangle$	$\langle\hat{n}_{s\uparrow}\rangle$
$\lvert\frac{1}{2}, \frac{1}{2}\rangle = \frac{1}{6}\{(2usd - sud + 2dsu - sdu - dus - uds)\uparrow\downarrow\uparrow +$	$\frac{5}{6}$	$\frac{5}{6}$	$\frac{1}{3}$
$(2sud - usd - dsu + 2sdu - dus - uds)\downarrow\uparrow\uparrow +$			
$(2uds + 2dus - sdu - dsu - sud - usd)\uparrow\uparrow\downarrow\}$			
$\lvert\frac{1}{2}, -\frac{1}{2}\rangle = \frac{1}{6}\{(usd + sud + dsu + sdu - 2dus - 2uds)\downarrow\downarrow\uparrow +$	$\frac{1}{6}$	$\frac{1}{6}$	$\frac{2}{3}$
$(sud - 2usd - 2dsu + sdu + dus + uds)\downarrow\uparrow\downarrow +$			
$(usd - 2sud + dsu - 2sdu + dus + uds)\uparrow\downarrow\downarrow\}$			

We now calculate $R_q^{M_{\Sigma^0}}$, beginning with the construction of the Σ^0 spin–flavor wavefunction. Unlike the Σ^*, which is a member of the symmetric baryon decuplet, the Σ^0 is in the mixed-antisymmetric octet and has a more complicated wavefunction. Table A.2 lists the Σ^0 spin–flavor wavefunctions and $\langle\hat{n}_{q\uparrow}\rangle$ for different M_{Σ^0}.

We use $\langle\hat{n}_{q\uparrow}\rangle$ to calculate the ensemble average of the polarization of Σ^0 particles originating from the three different flavors of quarks:

$$\begin{aligned}
\langle P_u^{\Sigma^0}\rangle &= \frac{\sum_{M_{\Sigma 0}}\langle\hat{n}_{u\uparrow}\rangle(\frac{M_{\Sigma 0}}{S_{\Sigma 0}})}{\sum_{M_{\Sigma 0}}\langle\hat{n}_{u\uparrow}\rangle} \\
&= \frac{\frac{5}{6}(1) + \frac{1}{6}(-1)}{\frac{5}{6} + \frac{1}{6}} \\
&= \frac{2}{3} \\
\langle P_d^{\Sigma^0}\rangle &= \frac{\sum_{M_{\Sigma 0}}\langle\hat{n}_{d\uparrow}\rangle(\frac{M_{\Sigma 0}}{S_{\Sigma 0}})}{\sum_{M_{\Sigma 0}}\langle\hat{n}_{d\uparrow}\rangle} \\
&= \frac{\frac{5}{6}(1) + \frac{1}{6}(-1)}{\frac{5}{6} + \frac{1}{6}} \\
&= \frac{2}{3}
\end{aligned}$$

$$
\begin{aligned}
\langle P_s^{\Sigma^0} \rangle &= \frac{\sum_{M_{\Sigma^0}} \langle \hat{n}_{s\uparrow} \rangle (\frac{M_{\Sigma^0}}{S_{\Sigma^0}})}{\sum_{M_{\Sigma^0}} \langle \hat{n}_{s\uparrow} \rangle} \\
&= \frac{\frac{1}{3}(1) + \frac{2}{3}(-1)}{\frac{1}{3} + \frac{2}{3}} \\
&= -\frac{1}{3}
\end{aligned}
$$

From Equation A.1, we obtain the following spin-transfer coefficients for Λ from Σ^0:

$$
\begin{aligned}
\langle P_u^{\Lambda} \rangle &= -\frac{1}{3} \langle P_u^{\Sigma^0} \rangle = -\frac{1}{3}(\frac{2}{3}) = -\frac{2}{9} \\
\langle P_d^{\Lambda} \rangle &= -\frac{1}{3} \langle P_d^{\Sigma^0} \rangle = -\frac{1}{3}(\frac{2}{3}) = -\frac{2}{9} \\
\langle P_s^{\Lambda} \rangle &= -\frac{1}{3} \langle P_s^{\Sigma^0} \rangle = -\frac{1}{3}(-\frac{1}{3}) = \frac{1}{9}
\end{aligned}
$$

A.2 Lambda produced from Ξ^0, Ξ^-

The Ξ^0 is a spin-1/2 particle with quark content = uss that decays to a Λ (spin-1/2) and π^0 (spin-0). By conservation of angular momentum, M_Λ is equal to M_{Ξ^0} throughout the decay process, i.e. $P_q^{\Xi^0} = P_q^{\Lambda}$.

We now construct the Ξ^0 spin–flavor wavefunction in order to calculate the production probabilities $R_q^{M_{\Xi^0}}$. Like the Σ^0, the Ξ^0 is a member of the baryon octet. Table A.3 lists the Ξ^0 spin–flavor wavefunctions and $\langle \hat{n}_{q\uparrow} \rangle$ for different M_{Ξ^0}.

Table A.3: Expectation values of the number of spin-up up and strange quarks in Ξ^0

Ξ^0 spin–flavor wavefunction	$\langle \hat{n}_{u\uparrow} \rangle$	$\langle \hat{n}_{s\uparrow} \rangle$
$\lvert \frac{1}{2}, \frac{1}{2} \rangle = \sqrt{\frac{1}{18}}(2s^\uparrow s^\uparrow u^\downarrow + 2u^\downarrow s^\uparrow s^\uparrow + 2s^\uparrow u^\downarrow s^\uparrow - s^\downarrow u^\uparrow s^\uparrow -$ $s^\uparrow s^\downarrow u^\uparrow - s^\downarrow s^\uparrow u^\uparrow - u^\uparrow s^\downarrow s^\uparrow - s^\uparrow u^\uparrow s^\downarrow - u^\uparrow s^\uparrow s^\downarrow)$	$\frac{1}{3}$	$\frac{5}{3}$
$\lvert \frac{1}{2}, -\frac{1}{2} \rangle = \sqrt{\frac{1}{18}}(s^\uparrow s^\downarrow u^\downarrow + s^\uparrow u^\downarrow s^\downarrow - 2u^\uparrow s^\downarrow s^\downarrow + s^\downarrow s^\uparrow u^\downarrow -$ $2s^\downarrow u^\uparrow s^\downarrow + u^\downarrow s^\uparrow s^\downarrow + s^\downarrow u^\downarrow s^\uparrow - 2s^\downarrow s^\downarrow u^\uparrow + u^\downarrow s^\downarrow s^\uparrow)$	$\frac{2}{3}$	$\frac{1}{3}$

Using the values of $\langle \hat{n}_{q\uparrow} \rangle$ obtained above, we calculate the ensemble average of the polarization of the Ξ^0:

$$
\begin{aligned}
\langle P_u^{\Xi^0} \rangle &= \frac{\sum_{M_{\Xi^0}} \langle \hat{n}_{u\uparrow} \rangle (\frac{M_{\Xi^0}}{S_{\Xi^0}})}{\sum_{M_{\Xi^0}} \langle \hat{n}_{u\uparrow} \rangle} \\
&= \frac{\frac{1}{3}(1) + \frac{2}{3}(-1)}{\frac{1}{3} + \frac{2}{3}} \\
&= -\frac{1}{3} \\
\langle P_d^{\Xi^0} \rangle &= \frac{\sum_{M_{\Xi^0}} \langle \hat{n}_{d\uparrow} \rangle (\frac{M_{\Xi^0}}{S_{\Xi^0}})}{\sum_{M_{\Xi^0}} \langle \hat{n}_{d\uparrow} \rangle} \\
&= 0 \\
\langle P_s^{\Xi^0} \rangle &= \frac{\sum_{M_{\Xi^0}} \langle \hat{n}_{s\uparrow} \rangle (\frac{M_{\Xi^0}}{S_{\Xi^0}})}{\sum_{M_{\Xi^0}} \langle \hat{n}_{s\uparrow} \rangle} \\
&= \frac{\frac{5}{3}(1) + \frac{1}{3}(-1)}{\frac{5}{3} + \frac{1}{3}} \\
&= \frac{2}{3}
\end{aligned}
$$

We previously determined that $\langle P_q^{\Xi^0} \rangle = \langle P_q^{\Lambda} \rangle$, so the spin-transfer coefficients for Λ particles produced from Ξ^0 are $\langle P_u^{\Lambda} \rangle = -\frac{1}{3}$, $\langle P_d^{\Lambda} \rangle = 0$, and $\langle P_s^{\Lambda} \rangle = \frac{2}{3}$.

The same calculation can be performed for the Ξ^-, which is identical to the Ξ^0 except for its quark content (quark content = dss). The spin-transfer coefficients for Λ particles produced from Ξ^- are $\langle P_u^{\Lambda} \rangle = 0$, $\langle P_d^{\Lambda} \rangle = -\frac{1}{3}$, and $\langle P_s^{\Lambda} \rangle = \frac{2}{3}$.

B Quark tracing in the Monte Carlo

In order to trace the struck quark through Monte Carlo events, the events must be generated with the JETSET switch MSTU(16)=2. The following are examples of events with MSTU(16)=1 and MSTU(16)=2, respectively.

Tracing OFF, MSTU(16)=1:

I	particle/jet		KS	KF	orig	p_x	p_y	p_z	E	m
4	e+		1	-11	1	-1.514	-0.667	11.262	11.383	0.001
5	(u)		13	2	0	1.964	0.432	16.227	16.351	0.006
6	(ud_0)		13	2101	2	-0.450	0.235	0.081	0.774	0.579
7	(u)	A	12	2	5	1.964	0.432	16.227	16.351	0.006
8	(ud_0)	V	11	2101	6	-0.450	0.235	0.081	0.774	0.579
9	(string)		11	92	7	1.514	0.667	16.308	17.125	4.959
10	(pi0)		11	111	9	1.143	0.582	9.025	9.117	0.135
11	(rho+)		11	213	9	0.131	-0.810	3.518	3.672	0.663
12	(rho-)		11	-213	9	0.237	0.357	1.094	1.454	0.857
13	p+		1	2212	9	0.003	0.537	2.671	2.881	0.938
14	gamma		1	22	10	0.804	0.385	5.843	5.911	0.000
15	gamma		1	22	10	0.338	0.197	3.182	3.206	0.000

Tracing ON, MSTU(16)=2:

I	particle/jet		KS	KF	orig	p_x	p_y	p_z	E	m
4	e+		1	-11	1	-1.514	-0.667	11.262	11.383	0.001
5	(u)		13	2	0	1.964	0.432	16.227	16.351	0.006
6	(ud_0)		13	2101	2	-0.450	0.235	0.081	0.774	0.579
7	(u)	A	12	2	5	1.964	0.432	16.227	16.351	0.006
8	(ud_0)	V	11	2101	6	-0.450	0.235	0.081	0.774	0.579
9	(string)		11	92	7	1.514	0.667	16.308	17.125	4.959
10	(pi0)		11	111	7	1.143	0.582	9.025	9.117	0.135
11	(rho+)		11	213	8	0.131	-0.810	3.518	3.672	0.663
12	(rho-)		11	-213	8	0.237	0.357	1.094	1.454	0.857
13	p+		1	2212	8	0.003	0.537	2.671	2.881	0.938
14	gamma		1	22	10	0.804	0.385	5.843	5.911	0.000
15	gamma		1	22	10	0.338	0.197	3.182	3.206	0.000

In both events, rows 10-13 (π^0, ρ^+, ρ^-, p) correspond to the primary particles produced from the string. In the first event with MSTU(16)=1, the parent row ("orig") of these primary particles is the row that contains the string. In the second event with MSTU(16)=2, the ends of the string are identified in the parents of the primary particles—the parent of the π^0 is the struck u quark (row seven), while the parent of the remaining particles is the $(ud)_0$ remnant (row eight). This additional information given when MSTU(16)=2 allows one to trace Λ particles by parent back to the struck quark.

Acknowledgments

It's been about a year since the original deadline for this thesis, and I think the time to stop revising has finally come. Many thanks to Dave Hertzog and Celia Elliott, the fearless leaders of the UIUC senior thesis class, for putting up with such extreme levels of procrastination and for sharing all their secrets about scientific communication and life in academia. Of course, none of this work would have been possible without the endless support and help of Gnome, an advisor in every sense of the word and beyond. Finally, thanks to the entire HERMES crew for being such wonderful people to hang around during my (short) career in nuclear physics. It's been a blast and a half; maybe I'll be back sometime...